Aus der

Berufsgenossenschaftlichen Unfallklinik

Klinik für Unfall- und Wiederherstellungschirurgie an der
Universität Tübingen

The effects of 3D-culture and stimulation with 5-Azacytidine and Vitamin C on HepG2 cells in culture

Inaugural-Dissertation
zur Erlangung des Doktorgrades
der Medizin

der Medizinischen Fakultät
der Eberhard-Karls-Universität
zu Tübingen

vorgelegt von
Grom-Baumgarten, Carl Ismail
2023

Dekan: Professor Dr. B. Pichler

1. Berichterstatter: Professor Dr. A. Nüssler
2. Berichterstatter: Professor Dr. N.P. Malek

Tag der Disputation: 14.11.2023

Table of Contents

TABLE OF CONTENTS 3

LIST OF FIGURES 6

LIST OF TABLES 6

1 INTRODUCTION 7

1.1 PHARMACOLOGICAL RESEARCH 7
1.1.1 DRUG DISCOVERY 7
1.1.2 PRECLINICAL AND CLINICAL DRUG DEVELOPMENT 7
1.1.3 *IN VIVO* RESEARCH 8
1.1.4 *IN VITRO* RESEARCH 9
1.1.5 CELL LINES IN HEPATOTOXICITY STUDIES 9
1.1.5.1 PRIMARY HUMAN HEPATOCYTES (PHH) 9
1.1.5.2 HEPATOMA CELLS LINES 10
1.1.5.2.1 HEPG2 CELL LINE 10
1.1.5.3 Other cell lines 14
1.1.6 EPIGENETIC MODIFICATION 11
1.1.7 EPIGENETIC MODIFICATION OF HEPATOMA CELL LINES 12
1.1.7.1 5-Azacytidine and Vitamin C 12
1.2 THE LIVER 12
1.2.1 ANATOMY 12
1.2.1.1 Liver histology 12
1.2.2 PHYSIOLOGY 14
1.2.2.1 AMMONIA DETOXIFICATION 14
1.2.2.2 BIOTRANSFORMATION 15
1.2.2.2.1 CYTOCHROME P450 ISOENZYMES 15
1.2.2.2.2 PHASE-II-ENZYMES 15
1.2.2.2.3 EXCRETION ENZYMES 16
1.2.3 DRUG INDUCED LIVER INJURY 16
1.3 LIVER CELL CULTURE 16
1.3.1 SANDWICH CULTURE 17
1.3.2 SCAFFOLDS 18
1.3.2.1 Cryogels 18
1.4 AIM OF THE STUDY 19

2 MATERIALS AND METHODS 20

2.1 MATERIALS 20
2.1.1 CONSUMABLES 20
2.1.2 CHEMICALS 20
2.1.3 EQUIPMENT 22
2.1.4 PROGRAMS 22
2.2 METHODS 22

2.2.1 CELL CULTURE 23
2.2.1.1 Trypsination and splitting 23
2.2.1.2 Stimulation with 5-AZA and Vitamin C 23
2.2.2 SANDWICH CULTURE 23
2.2.2.1 Isolation of rat tail collagen 23
2.2.2.2 Preparation of Sandwich culture 24
2.2.3 PREPARATION OF CRYOGELS 24
2.2.3.1 Creation of Scaffolds 24
2.2.3.2 Cutting and sterilization of scaffolds 26
2.2.3.3 Seeding of Cells on Scaffolds 26
2.2.3.3.1 Surface Seeding 27
2.2.3.3.2 Orbital Seeding 27
2.2.4 MICROSCOPY 27
2.2.4.1 Pore diameter measurement 27
2.2.4.2 Hoechst Staining 28
2.2.4.3 Calcein AM Staining 28
2.2.4.4 SRB Staining 28
2.2.5 FUNCTIONAL ASSAYS 28
2.2.5.1 AMMONIA DETOXIFICATION 29
2.2.5.2 CYP ACTIVITY ASSAYS 29
2.2.5.3 PHASE II MEASUREMENT 30
2.2.5.3.1 Uridine diphosphate glucoronosyltransferase (UGT) measurement 30
2.2.5.3.2 Glutathione S-transferase (GST) activity measurement 31
2.2.5.4 EFFLUX ASSAYS 31
2.2.6 RESAZURIN CONVERSION ASSAY 31
2.2.7 RNA ISOLATION 32
2.2.7.1 CDNA SYNTHESIS 33
2.2.8 PCR 33
2.2.9 GEL ELECTROPHORESIS 33
2.3 STATISTICAL ANALYSIS 34

3 RESULTS 35

3.1 SCAFFOLD OPTIMISATION / CHARACTERISATION 35
3.1.1 SCAFFOLD COMPOSITION 35
3.1.2 PORE SIZE MEASUREMENTS 37
3.1.3 SUMMARY OF THE SCAFFOLD CREATION RESULTS 38
3.1.4 SCAFFOLD SEEDING 39
3.1.5 CELL MORPHOLOGY 40
3.2 FUNCTIONAL TESTS 40
3.2.1 AMMONIA DETOXIFICATION 41
3.2.2 CYP ACTIVITY 43
3.2.3 UGT / GST 46
3.2.4 EFFLUX ASSAYS 47
3.3 PCR 49
3.3.1 PREPARATORY TESTS FOR PCR 49
3.3.2 PCR RESULTS 50

4 DISCUSSION 53

4.1 LIMITATIONS OF METHODS 58

4.2 OUTLOOK 60

5 SUMMARY 62

6 ZUSAMMENFASSUNG 64

7 LIST OF ABBREVIATIONS 65

8 APPENDICES 68

8.1 PRIMERS USED: 68

9 REFERENCES 70

ERKLÄRUNG ZUM EIGENANTEIL 80

List of figures

FIGURE 1: THE DRUG DEVELOPMENT PROCESS ("THE DRUG DEVELOPMENT PROCESS," 2018) 7
FIGURE 2: IN CULTURE, PHH RAPIDLY LOSE FUNCTION AND ZONAL POLARITY 10
FIGURE 3: LIVER ORGANIZATION ON A MICROSCOPIC LEVEL. 13
FIGURE 4: PREPARATION OF SANDWICH CULTURE 24
FIGURE 5: SCAFFOLD CREATION 25
FIGURE 6: SCAFFOLD CREATION WORKFLOW 26
FIGURE 7: SCAFFOLDS WITHOUT (LEFT) AND WITH (RIGHT) 24 HOURS OF PRE-INCUBATION IN MEDIUM WITH FBS 26
FIGURE 8: WORKFLOW OF THE STIMULATION AND TESTING 29
FIGURE 9: STANDARD CURVES OF RESAZURIN CONVERSION AFTER 60 AND 150 MINUTES OF INCUBATION 32
FIGURE 10: MICROSCOPY OF THE TOP OF SCAFFOLDS FROM COMPOSITION 1 35
FIGURE 11: MICROSCOPY OF CROSS SECTIONS OF SCAFFOLDS FROM COMPOSITION 2 36
FIGURE 12: MICROSCOPY OF THE TOP OF SCAFFOLDS FROM COMPOSITION 3 36
FIGURE 13: MICROSCOPY OF THE TOP OF SCAFFOLDS FROM COMPOSITION 4 37
FIGURE 14: PORE SIZE MEASUREMENT OF SCAFFOLDS FROM COMPOSITION 1-4 37
FIGURE 15:MICROSCOPY OF DIFFERENT SEEDING TECHNIQUES 39
FIGURE 16: CELL MORPHOLOGY OF HEPG2 CELLS IN 2D 40
FIGURE 17: UREA PRODUCTION OVER 24 HOURS IN A BASIC SOLUTION 41
FIGURE 18: UREA PRODUCTION OVER 24 HOURS IN A SOLUTION CONTAINING AMMONIUM CHLORIDE 41
FIGURE 19: UREA PRODUCTION IN A SOLUTION CONTAINING AMMONIUM CHLORIDE AS WELL AS ORNITHINE 42
FIGURE 20: CYP1A2 ACTIVITY 43
FIGURE 21: CYP2C9 ACTIVITY 44
FIGURE 22: CYP3A4 ACTIVITY 45
FIGURE 23: UGT ACTIVITY AFTER 30 AND AFTER 60 MINUTES 46
FIGURE 24: GST ACTIVITY AFTER 30 AND AFTER 60 MINUTES 46
FIGURE 25: MRP1 ACTIVITY AFTER 30 AND AFTER 60 MINUTES 47
FIGURE 26: MDR1 ACTIVITY AFTER 30 AND AFTER 60 MINUTES 48
FIGURE 27: RNA YIELD FROM CELLS CULTURED ON DIFFERENT MECHANICAL SUBSTRATES. 49
FIGURE 28: GEL ELECTROPHORESIS OF GAP-DH AND HPRT 49
FIGURE 29: EXPRESSION LEVELS OF CYP 1A2 AND CYP 2C9 50
FIGURE 30: EXPRESSION LEVELS OF UGT 51
FIGURE 31: EXPRESSION LEVELS OF MRP1 AND MDR1 51
FIGURE 32: EXPRESSION LEVELS OF CPS 52

List of tables

TABLE 1: LIST OF CONSUMABLES 20
TABLE 2: LIST OF CHEMICALS 21
TABLE 3: LIST OF EQUIPMENT 22
TABLE 4: LIST OF PROGRAMS 22
TABLE 5: LIST OF READY KITS USED 22
TABLE 5: TABLE OF SCAFFOLD COMPOSITIONS AND THE CONCENTRATION OF CONTENTS 25
TABLE 6: CONTENTS OF AMMONIA DETOXIFICATION TEST SOLUTIONS 29
TABLE 7: CONTENTS OF CYP TEST SOLUTION 30

1 Introduction

1.1 Pharmacological research

The development of drugs for the treatment of human diseases is a very long and thorough process. On average, only one in five to ten thousand possible drug candidates reaches approval by the US Food and Drug Administration (Giri *et al.*, 2011)

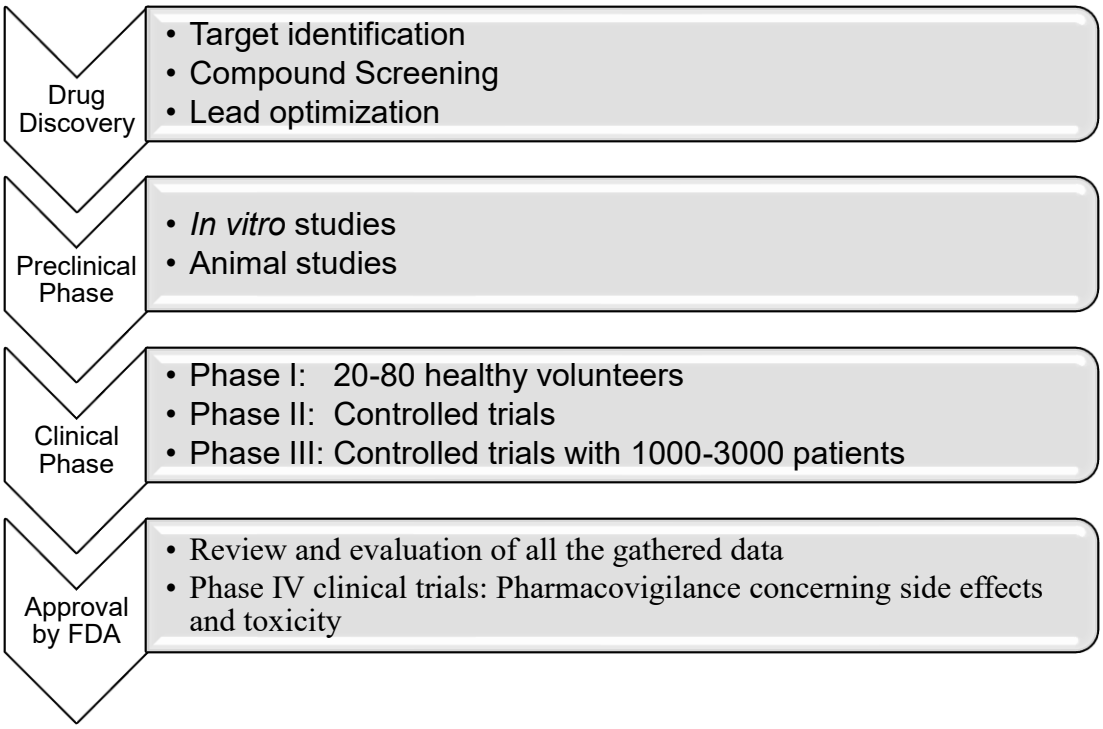

Figure 1: The drug development process (Brodniewicz et al.*, 2018)*

1.1.1 Drug discovery

The first step on this path is drug discovery, in which compounds that interact with central targets of the disease are identified. Based on detailed knowledge of these targets, large-scale screening of compounds is carried out to find those that interact the most favorable. The ones that do are then further modified to either improve the desired effect or reduce unwanted interactions (Brodniewicz *et al.*, 2010).

1.1.2 Preclinical and clinical drug development

When a compound has been identified and modified, it progresses to preclinical testing. There, it is investigated regarding pharmacokinetics, pharmacodynamics and overall effect on the organism, especially toxicity and dosing (Fox *et al.* 2002). Methods in the preclinical phase include cell culture and molecular methods (*in vitro*), animal testing (*in vivo*) and increasingly computational modelling (*in silico*) approaches to ensure that the

compound is safe for human testing (Jankovic *et al.* 2019; Sinha *et al.*, 2019). *In vivo* experiments are currently the only reliable and approved way to investigate a drug for teratogenicity and carcinogenesis. Before a compound is cleared for clinical testing, its toxicity needs to be investigated in two mammalian species, one of them non-rodent ("Directive 2001/83/EC," 28/11/2001).

The clinical stage of drug development begins with phase I clinical trials, the dose-finding phase. Here, the compound is given to 20-80 healthy volunteers, who are then closely monitored regarding toxicity, side effects, pharmacokinetics and pharmacodynamics (Fox *et al.*, 2002). In phase II clinical trials, the compound is administered to 100-300 patients with the disease it is intended to treat to show its efficacy compared to placebo.

The last clinical phase before approval is sought from regulatory bodies are the phase III trials, where the compound is given to 1000-3000 patients and compared to existing treatments. Drug interactions, side effects and dosage are also evaluated in this step.

After phase III, the entirety of the data that has been collected up to this point is compiled and reviewed by the researchers, a process that can take several years. It is then presented to the regulatory bodies. In the European Union this is the European Medicines Agency (EMA), in the United States this is the Federal Drug Administration (FDA). If the evidence regarding nontoxicity, efficacy and the properties of the compound is deemed sufficient and the compound is deemed safe, it is granted approval and can be manufactured for the market (Fox *et al.*, 2002).

In phase IV, which is continuously done after regulatory body approval, the drug and the patients taking it are constantly monitored for side effects and long-term effects (pharmacovigilance) (Fox *et al.*, 2002). Even after approval has been granted, a drug can be withdrawn or further restricted due to unforeseen toxicity or interactions. Major causes for drug withdrawal are liver toxicity, immune-related side-effects, and an increase of cardiovascular risk (Onakpoya *et al.*, 2011).

1.1.3 *In vivo* research

The practice of using laboratory animals to test the safety and efficacy of a treatment is not a new one, it has led to such immense breakthroughs such as the use of insulin in the treatment of diabetes (Vecchio *et al.* 2018), the diphtheria antitoxin (Grundbacher, 1992) and a large number of surgical procedures including organ transplantation (Song *et al.*, 2013). Despite their accomplished history, *in vivo* studies face immense challenges in modern drug development. Besides concerns for the wellbeing and safety of the animals,

the limitations of extrapolating animal test data to human applications are becoming more apparent (Leist *et al.*, 2013). *In vivo* experiments are currently the only approved and reliable way to investigate a drug for chronic toxicity, teratogenicity and carcinogenesis before human application in clinical trials (Fox *et al.*, 2002).

1.1.4 *In vitro* research

In vitro research summarizes all approaches being done in the laboratory, mainly cell culture and molecular methods. It has been used for a long time to investigate the behavior of cells and molecules under standardized conditions (Dambach *et al.,* 2005). Cell culture experiments are performed by culturing one or several types of cells under sterile conditions and observing their reaction to certain conditions, such as stress, chemical exposure, or hypoxia. When performed with human cells, they can help to predict the effects of drugs on human tissue, a shortfall of animal testing (Dambach *et al.*, 2005).
In the drug development process, *in vitro* research is used to gather as much data as possible about a compound before the *in vivo* application in animal models (Jankovic *et al.*, 2019). This helps in narrowing down the number of candidates that move into animal testing, but also provides insight into the effects of the tested compounds on cells in different concentrations and under varying conditions (Ghanemi, 2015). A challenging part when bridging the gap between cell culture and animal testing is *in vitro* to *in vivo* extrapolation (IVIVE), because even the more sophisticated cell culture approaches lack the complexity of *in vivo* conditions (Louisse *et al.*, 2010). Thus, a diligent choice of cell line and culture conditions is crucial to ensure that the data provided is reliable, as it is used to further refine the following steps in the drug development process (Ghanemi, 2015).

1.1.5 Cell lines in hepatotoxicity studies

1.1.5.1 Primary human hepatocytes (pHH)

Primary human hepatocytes are the gold standard for *in vitro* liver toxicity studies. They are the only model of *in vitro* studies for drug development currently approved by the US-American FDA and have been shown to possess stable levels of liver-specific enzyme activity for several days after isolation, which can be used in the investigation of the metabolism of rapidly-clearing drugs as well as acute liver injury mechanisms (Kidambi *et al.*, 2009).

However, it has also been shown that directly after isolation, pHH begin to rapidly de-differentiate, losing their enzyme function, morphology, and their characteristic zonal polarization (Godoy *et al.*, 2009; Treyer *et al.*, 2013). As Figure 2 shows, pHH in culture lose their morphological features and flatted, when cultured in 2D. Adding media substrates and coating the cell culture plates with collagen have aided in maintaining hepatocyte function longer (Koike *et al.,* 1996; Kost *et al.*, 1991). However, it is currently not possible to halt or even significantly slow this deterioration to a point where pHH can reliably be cultured over what is required for long-term study of liver toxicity (Guguen-Guillouzo *et al.*, 2010).

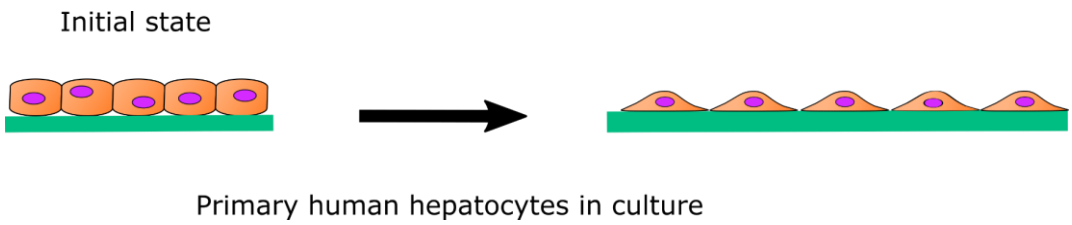

Figure 2: In culture, pHH rapidly lose function and zonal polarity and take on a flattened morphology (after Treyer et al.*, 2013)*

Other major drawbacks of pHH include their scarce availability of the cells as well as limited predictability of the viability of cells after isolation, especially if the cells have to be shipped or the donor tissue is of poor quality (Berendsen *et al.*, 2011; Green *et al.*, 2017).

1.1.5.2 Hepatoma cells lines

1.1.5.2.1 HepG2 cell line

The HepG2 cell line was first described in 1979 by Aden *et al.* It was isolated from the liver of a 15-year old boy who suffered from hepatoblastoma, which had developed independently of hepatitis infection (Aden *et al.* 1979). It has been shown in numerous studies to have residual activity of liver specific enzymes, albeit on much lower levels than pHH (Aninat *et al.*, 2006; Wilkening *et al.* 2003). Among these is the secretion of plasma proteins typically secreted by the liver, such as albumin and transferrin (Bouma *et al.*, 1988). Additionally, the cells maintain a comparatively high morphological differentiation (Wilkening *et al.*, 2003).

HepG2 cells are often used in studies in place of pHH, due to the lack of inter-individual variation and the general availability (Wilkening *et al.*, 2003). In addition to this, several studies have investigated the potential of increasing the liver-like function of HepG2 by

means of changing culture conditions, both by medium additives as well as by 3D culture (Luckert *et al.*, 2017; Ramaiahgari *et al.*, 2014).

Ramaiahgari *et al.* found an increase of activity of several key enzymes when HepG2 cells were cultured over 21 days in 3D culture (Ramaiahgari *et al.*, 2014) However, Luckert *et al.* found this to be mainly a function of culture-time and less of 3D culture itself. Despite this, they reported finding an increase in Cytochrome p450 (CYP) 1A2 activity in 3D culture (Luckert *et al.*, 2017).

We chose the HepG2 cell line for our experiments, as it represents a very well-described, stable cell line that has a residual activity of most liver-specific enzymes of interest to our study. Over the last decades, several other hepatoma cell lines for the study of *in vitro* liver toxicity have been described, among them include Huh-7, HepaRG and HLE. In addition to this, attempts have been made to create induced pluripotent stem cells that can mimic hepatocyte function while circumventing major drawbacks like scarce availability and rapid deterioration (Castell *et al.,* 2006).

1.1.6 Epigenetic modification

With pHH in scarce supply, many attempts have been made to alter the epigenetics of more widely available cell lines, such as hepatoma cells.

Epigenetics are an integral part of regulating cell specialization and activity throughout the human body. They enable cells with a (near) identical genome to fulfill a variety of different functions and adapt to their role in physiological processes. Several different epigenetic mechanisms are known. On the level of the gene, methylation of nucleotides, most notably the methylation of cytosine in position 5 (5mC) at the promotor leads to the repression and inactivation of the gene in question. Other mechanisms include ribonucleic acid (RNA) modification, microRNAs and other covalent modifications, such as acetylation and ubiquitination (Dupont *et al.*, 2009).

In many cancers the epigenetics change drastically over the progression from physiological tissue to cancer, deactivating or mutating tumor-suppressor genes like *p53* and activating proto-oncogenes. Drugs that can partially or fully reverse these changes have been used to treat certain cancers successfully (Kanwal *et al.*, 2012).

1.1.7 Epigenetic modification of hepatoma cell lines

1.1.7.1 5-Azacytidine and Vitamin C

5-Azacytidine (5-Aza) demethylates the C-5 position of cytosine, creating 5-hydroxymethyl cytosine (5hmC), leading to the reversing of the repression of the affected gene. The mechanism of this is still a subject of study, although it has been shown that it is dependent on the activity of ten-eleven-transferases (TETs) in *in vitro* studies (Ruoß *et al.*, 2019; Sajadian *et al.*, 2016; Seeliger *et al.*, 2013).

Vitamin C (ascorbic acid) is an essential molecule for the synthesis of collagen fibers, where it hydroxylates the Proline side chain. It has been demonstrated that Vitamin C can enhance the effects of 5-Aza in reversing the hypermethylation of tumor suppressor genes (Sajadian *et al.*, 2016).

Co-stimulation of HepG2 cells with 5-Azacytidine and Vitamin C has been shown to increase the activity of several liver-specific enzymes, such as the cytochrome p450 enzymes CYP2C9, CYP2D6 as well as increase expression of several genes like CYP1A2 and CYP2C9, albeit on a much lower level than in pHH and to increase the expression of epithelial-like markers such as HNFα (Ruoß *et al.*, 2019).

5-Azacytidine is known to induce demethylation in genes in several hepatocellular carcinoma cell lines (Huh-7, HLE and HLF) through the ten-eleven translocation protein 2 (TET2) (Sajadian *et al.*, 2015). This effect was further enhanced in Huh-7 and HLE cell culture by the addition of Vitamin C (Sajadian *et al.,* 2016). The treatment was also shown to partially reverse EMT in HepG2 cells as data published by Ruoß *et al.* showed (Ruoß *et al.*, 2019).

1.2 The Liver

1.2.1 Anatomy

Located in the upper right abdomen, the liver weighs approximately 1.4-1.8 kg and fulfills a central role in energy and substrate metabolism, detoxification and the first-pass-effect. (Aumüller, 2010, pp. 656-658).

1.2.1.1 Liver histology

The microscopic unit of the liver is the liver lobule. The entire parenchyma of the liver is made up of these hexagonal structures, which are approximately 1 mm in diameter and 2 mm high. At the center of each lobule is the central vein, which ultimately drains the blood to the liver veins. On each of the corners is a triad of branches of bile duct, portal

vein and hepatic artery, the portal triad. The function of the portal triad is the delivery of both highly oxygenated blood from the hepatic artery and highly nutritious blood from the portal vein, as well as the drainage of bile to the gall bladder (Aumüller, 2010, pp. 660-664).

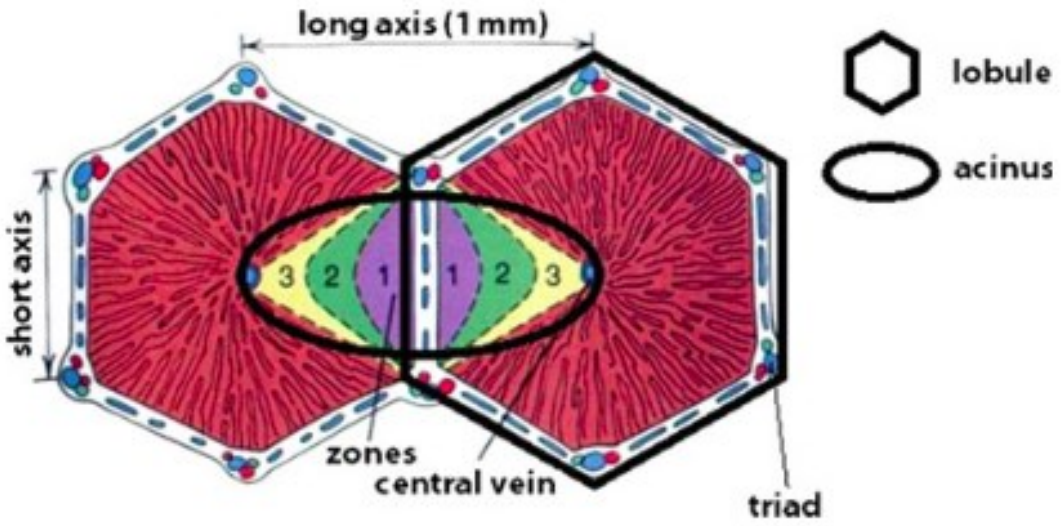

Figure 3: Liver organization on a microscopic level. Nutrient and oxygen gradients exist depending on the distance from central vein and allow for zonal specialization of hepatocytes. The liver acinus is a histological unit of organization as well as a functional one, while the acinus is a purely functional one. Picture from Godoy et al. *Article published under creative commons license Creative Commons CC-BY-NC for non-commercial use, distribution, and reproduction in any medium (Godoy* et al.*, 2013)*

The functional unit of the liver is the liver acinus, which has a triangular shape and spans between two portal triads and one central vein. The blood flows from the portal triads to the central vein, changing its composition along the way due to the metabolic activity of the hepatocytes (Aumüller, 2010, p. 661).

Due to the gradients in oxygen and nutrients, the cells show a high level of zonal differentiation. In the periportal zone there is a high partial pressure of oxygen, and the cells perform tasks of the carbohydrate, amino acid, and lipid metabolism as well as plasma protein synthesis. The cells in the perivenous zone have much less oxygen and specialize in the detoxification of xenobiotics and other substances that need to be excreted. Zonal differentiation is a key mechanism of liver functionality, allowing for a myriad of different tasks being performed simultaneously. Liver toxicity becomes first apparent in the perivenous zone (Kietzmann, 2017).

Within the microscopic architecture of the lobule, the blood from the portal triad flows by a fenestrated membrane, the sinusoidal membrane, allowing the blood plasma to enter the space of Dissé, but keeping blood cells out. The hepatocytes, which make up around

60% of the cells in the liver, can freely access the plasma in the space of Dissé and interact with it. Their apical side faces away from the sinusoids and forms the bile canaliculi around tight junctions between neighboring hepatocytes. The basolateral sides face the space of Dissé and interact with the plasma in it, exchanging nutrients and metabolites.
Alongside the hepatocytes, other non-parenchymal cells are present in the liver. The sinusoidal endothelial cells form the membrane separating the space of Dissé from the blood (Aumüller, 2010, pp. 661-662). Kupffer cells fulfill a function as tissue macrophages in the liver and are an important part of the immune response in liver inflammation by secreting pro-inflammatory cytokines like tumor necrosis factor α (TNFα) (Roberts *et al.*, 2006). Other immune cells such as pit cells (specialized lymphocytes), granulocytes and dendritic cells can be found in the liver as well (Aumüller, 2010, p. 662). Hepatic stellate cells are located in the space of Dissé and act as storage cells for lipophilic substances, such as vitamin A. In chronic liver disease they undergo a phenotypical change and secrete extracellular matrix proteins, which can lead to fibrosis (Bataller *et al.*, 2005). A small portion of cells in the liver are cholangiocytes, which line the biliary tract (Aumüller, 2010, p. 662).

1.2.2 Physiology

The liver is a vital organ, performing a central role in glucose, protein and lipid homeostasis, as well as plasma protein synthesis and the biotransformation of xenobiotics and endogenous substances (Aumüller, 2010, pp. 660-664).

1.2.2.1 Ammonia detoxification

A key function of the hepatocytes is the detoxification of ammonia to urea (Horn, 2009). Ammonia is a by-product of the protein metabolism of every cell in the body and it causes irreversible neurological damage when it accumulates in the plasma (Horn, 2009). In the Urea cycle, ammonia is metabolized by several key enzymes including arginase, and carbamoyl phosphate synthetase 1 (CPS1), which is the pacemaker enzyme (Horn, 2009). This process is located in the cytosol and mitochondria of the hepatocytes and insufficient detoxification leads to hepatic encephalopathy (Horn, 2009).
Ammonia detoxification is present, albeit very low in HepG2 cells compared to pHH (Cipriano *et al.*, 2017).

1.2.2.2 Biotransformation

One of the most important functions of the liver is the metabolism of potentially harmful substances, both foreign and from the body itself. This process, known as biotransformation occurs in the hepatocytes in three phases (Horn, 2009).

1.2.2.2.1 Cytochrome p450 (CYP) isoenzymes

Phase I, catalyzed by enzymes of the CYP family, includes oxidative, reductive and hydrolytic reactions to add functional groups (-OH, -SH or $-NH_2$) (Horn, 2009). Several enzymes have been identified as being of key importance to the development and metabolism of drugs.

CYP3A4 is directly involved in the metabolism up to 60% of the prescription drugs currently used. Furthermore, it can be inhibited and induced by many widely available substances, such as grapefruit juice and St John's wart as well as being a key enzyme in drug interactions (Dresser *et al.,* 2000).

CYP1A2 metabolizes several commonly used drugs, among them tricyclic antidepressants and the anticancer drug Tamoxifen (Lim *et al.*, 2011; Zhou *et al.,* 2010).

CYP2C9 also metabolizes Tamoxifen, as well as many other drugs like Warfarin and Diclofenac (Lim *et al.*, 2011).

1.2.2.2.2 Phase-II-enzymes

Phase I paves the way for phase II, in which the functional groups are modified by addition of molecules such as glucuronides and sulfate esters to increase the water solubility of the compound (Wilkening *et al.*, 2003). Two of the most important groups in drug metabolism are the glutathione-S-transferase (GST) and uridine diphosphate glucoronosyl-transferase (UGT) groups (Jancova *et al., 2010*). These enzymes are expressed at high levels in pHH; however, they are also present in HepG2. While the activity of UGT is much lower in HepG2 compared to pHH, the activity of several enzymes from the GST-group, among them GSTα1 have been described as higher in HepG2 (Westerink *et al.*, 2007). Additionally, increased GST activity is linked to chemotherapeutic resistance (Hayes *et al.*, 1995).

1.2.2.2.3 Excretion enzymes

Phase III excretion enzymes consist of transporters of the Antigen-Binding-Cassette (ABC) family, that transport the conjugated molecules through either the apical membrane into the bile canaliculi or the basal membrane into the bloodstream (Treyer *et al.*, 2013). Major proteins with this function are Multidrug Resistance Protein 1 (MDR1) and Multidrug resistance related Protein 1 (MRP1). MDR1 and MRP1 are transmembrane proteins that serve to translocate molecules via membranes (Dean *et al*, 2001; Kumar *et al.*, 2019; Lu *et al.*, 2015). *MRP1* (*ABCC1*) and *MDR1* (*ABCB1*) gene overexpression occurs in a variety of cancer cells and is associated with resistance against chemotherapy (Dean *et al.*, 2001).

1.2.3 Drug induced Liver injury

Drug induced liver injury (DILI) represents by far the leading cause of acute liver failure (ALF) in countries such as Germany and the US, with 46% of cases of ALF caused by Acetaminophen-mediated toxicity and a further 11% by toxicity from other drugs (Stravitz *et al.,* 2019). While the mechanism of the toxicity of some substances like acetaminophen (APAP) is well understood and predictable, other drugs cause idiosyncratic and very unpredictable effects (David *et al.*, 2010).

The main limitation of pHH in 2D is a rapid deterioration in function and loss of their distinct morphology over the span of days. Other cell lines such as HepG2 exhibit steady, albeit low activity of liver-specific enzymes, but are more readily available and generally easier to culture. Their low activity makes them unsuited for use in comprehensive toxicity testing, although specific aspects, such as cholestatic DILI can already be investigated, as this form of DILI does not require metabolic activity on the level of pHH (Sison-Young *et al.*, 2017).

1.3 Liver cell culture

Liver cells *in vivo* express a specific pattern of surface molecules on their apical, basolateral, and sinusoidal sides, leading to a high level of polarization. In two-dimensional cell culture, they lose their polarity and rapidly deteriorate. This is due to the liver cells changing their gene expression toward proliferation and losing metabolic function in the process. The aim of current research is hence to maintain polarity and

function by culturing the hepatocytes in a more physiological environment (Elaut *et al.*, 2006).

To circumvent the loss of functionality and polarity, several culture-based strategies have been established: **Perfused liver slices** resemble *in vitro* conditions closely because they contain all the cells of the liver in their physiological configuration, but they are difficult to handle and quickly lose function as well (Bessems *et al.*, 2006). **In microfluidic "organs-on-a-chip**", a small number of functional cells is seeded on a plate with several channels, through which fluids are pumped and the metabolites analyzed (Kimura *et al.*, 2018). This approach has been successfully applied to models of lung and kidney tissue, however, due to the complex organization of the liver this technology is still in its infancy (Beckwitt *et al.*, 2018). **Hepatospheres** are formed by conglomeration of hepatocytes when their adherence to other molecules is prohibited. Within them, liver cells show higher polarity and bile canaliculi formation as well as an increase in cell-cell contact (Hussain *et al.*, 2018). Another approach to more closely mimic *in vivo* conditions is co-culture, in which hepatocytes and several types of non-parenchymal cells (NPC) are cultured together. This has been successfully done with Kupffer cells, stellate cells, and hepatic sinusoidal cells to name a few (Gebhardt *et al.*, 2003).

1.3.1 Sandwich culture

The simplest of three-dimensional methods is the sandwich culture. Here, the cell culture plate is coated in sterile collagen, which is left to polymerize. The cells are seeded on top of the polymerized collagen, left to adhere, and then covered with another layer of collagen or other basal-membrane-like substances (e.g. Matrigel) (Hughes, *et al., 2010)*. It has been demonstrated that this allows the cells to retain some of their functions for longer, thus staving off dedifferentiation. While this by no means is the be-all-end-all of 3D culture, it serves as a baseline to compare other methods to, as it is easy to reproduce and standardize across labs.

Collagen sandwich culture is a well-established method, mainly for culturing pHH, where it has been demonstrated to help maintain structural characteristics of pHH and a higher activity of liver-specific functions compared to regular 2D culture (Dunn *et al.*, 1989) and is commonly used as a comparison method when investigating more complex culturing techniques (Nagaki *et al.*, 2001).

The culturing of HepG2 in collagen sandwich culture was investigated in a paper published in 2016 by Luckert *et al.*, in which the activity of several CYPs as well as the

changes in gene expression over 21 days were described (Luckert *et al.*, 2017). A similar approach to the collagen sandwich is the collagen gel, in which the cells are immersed in the collagen before it polymerizes (Godoy *et al.,* 2010).

1.3.2 Scaffolds

Scaffolds are porous structures that allow cultured hepatocytes to interact with a three-dimensional environment and other cells. This culture technique has been shown to improve functions in hepatocytes, such as plasma protein synthesis and biotransformation capability as well as prolong them. The main techniques for scaffold creation are 3D printing, polymerization of organic or non-organic materials and electro-spinning (Chua *et al.*, 2005; Zhu *et al.*, 2016). Decellularized liver tissue can be classified as a scaffold as well, albeit a natural one (Pan *et al.*, 2011). A major factor in scaffold quality is the porosity. The more porous the scaffold is, the better cells can migrate into the center of the scaffold and be supplied by nutrients there. At the same time, a higher porosity results in less mechanical stability, which makes using it for culturing harder (Hollister, 2005).
For pHH, fairly easily manufactured 3D culture techniques such as hydrogels and spheroid culture have been shown to extend biotransformation and secretion over a longer period of time than 2D culture sources (Prestwich, 2008; Wang *et al.*, 2020), however, they suffer from several key drawbacks such as poor transfer of nutrients and medium (Godoy *et al.*, 2013).
More complex scaffolds can be created by several methods, such as 3D-printing, cryogels and electrospinning and have shown promise for cell culture application in the cultivation of pHH (Brown *et al.*, 2018; Damania *et al.*, 2018; Jain *et al.*, 2015; Kizawa, *et al.,* 2017). Similarly, for HepG2, a much more robust and readily available cell line, an increase in liver-like functionality was shown in 3D culture (Wei *et al.*, 2020). Especially for urea and albumin production, which can readily be determined in the supernatant, several studies were able to show an increase for HepG2 cultured in 3D (Jain *et al.*, 2015; Zhang *et al.*, 2016). 3D cell culture can be combined with continuous-flow techniques and co-culture with hepatic NPCs (Kimura *et al.*, 2018).

1.3.2.1 Cryogels

Cryogels are one of the techniques to create a scaffold quickly and comparatively inexpensively. One of their main advantages is, that single components can be adjusted or exchanged according to the experimental setup and the cells (Hixon *et al.,* 2017)

Cryogels are created by freezing a solution of proteins and cross-linkers while it freezes. The mixture cross-links around the forming ice crystals and creates an interconnected network of pores. This network allows cells to diffuse deeper into the scaffold and form cell-cell connections inside the scaffold (Hixon *et al.,* 2017). In our scaffold, the main components of the extracellular matrix are Poly-(2-hydroxyethyl-methacrylat) (pHEMA) as a structural element as well as collagen and gelatin as naturally occurring proteins to mimic better the physiological composition.

Biocompatible monomers and polymers, such as poly (lactic-co-glycolic acid) (PLGA), poly (glycolic acid) (PGA), and Poly(hydroxyethyl)methacrylate (pHEMA) have been used successfully in creating for several years (Mikos *et al.*, 2000; X. Wang *et al.*, 2020). pHEMA was developed in 1953 for the development of contact lenses and optical implants (Wichterle *et al.*, 1960). Apart from its use as a scaffold component it is used in cell culture flasks, where it prevents cell adherence to the walls, which is why scaffolds containing it require a protein component such as collagen for cells to adhere to the scaffold matrix (Stol *et al.*, 1985). pHEMA-based scaffolds have successfully been established for several cell types, such as osteoblasts, muscle cells and corneal cells (Häussling *et al.*, 2019; Kilic *et al.*, 2019; Stol *et al.*, 1985). Another major group of materials is biological materials such as rat tail collagen, alginate, and cold fish gelatin, which are generally non-toxic and have been used in a variety of cell-culture methods including hydrogels, sandwich and cryogels (Bachmann *et al.*, 2015; Brown *et al.*, 2018; Dunn *et al.*, 1989).

1.4 Aim of the study

This study aims to investigate the following:

1. The effect of 3D culture on the metabolic activity and gene expression in HepG2 cells
2. The effect of sandwich culture on the metabolic activity and gene expression in HepG2 cells
3. The combined effect of either culture type in combination with stimulation with 5-Azacytidine and Vitamin C on the metabolic activity and gene expression in HepG2 cells
4. The characterization of several scaffolds using hydrogel polymerization with pHEMA, Bis-acrylamide, collagen, and gelatin.

2 Materials and methods

2.1 Materials

2.1.1 Consumables

Material	Supplier
Cellstart Cell Culture Flasks 25, 75 and 175 cm^2	Greiner Bio - One, Frickenhausen, Germany
Cellstart Cell Culture Plates 24, 48 and 96 wells	Greiner Bio - One, Frickenhausen, Germany
Costar Stripette 5, 10, 25 and 50 ml	Corning, Corning, USA
Falcon 15 ml centrifuge tubes	Sigma Aldrich Chemie, Steinheim, Germany
Falcon 50 ml centrifuge tubes	Sigma Aldrich Chemie, Steinheim, Germany
Falcon Cell Culture Plates 6 wells	Becton, Dickinson & Co., Franklin Lakes, USA
Pipette Tips 20, 200, 1000 µl	Biozym Scientific, Hessisch Oldendorf Sarstedt, Germany
Syringe 2 ml	B. Braun AG, Melsungen, Germany

Table 1: List of Consumables

2.1.2 Chemicals

3,3'-Methylene-bis(4-hydroxycoumarin)	Sigma Aldrich Chemie, Steinheim, Germany
4-Methylumbelliferone	Sigma Aldrich Chemie, Steinheim, Germany
5-Azacytidin (5-Aza)	Sigma Aldrich Chemie, Steinheim, Germany
5-Carboxyfluorescein (5-CF)	Sigma Aldrich Chemie, Steinheim, Germany
5(6)-Carboxy-2',7'-dichlorofluorescein diacetate (CFDA)	Sigma Aldrich Chemie, Steinheim, Germany
7-Benzyloxy-4(trifluoromethyl)coumarin (BFC)	Sigma Aldrich Chemie, Steinheim, Germany
7-Ethoxycoumarin (ECOD)	Sigma Aldrich Chemie, Steinheim, Germany
7-Hydroxy-4(trifluoromethyl)coumarin (HFC)	Sigma Aldrich Chemie, Steinheim, Germany
Acetic Acid	VWR, Leuven, Belgium
Acetonitrile	Carl Roth, Karlsruhe, Germany
Agarose	Carl Roth, Karlsruhe, Germany
Ammonium chloride (NH_4Cl)	Carl Roth, Karlsruhe, Germany
Ascorbic Acid-2-Phosphate (Vitamin C)	Carl Roth, Karlsruhe, Germany
Boric Acid	Carl Roth, Karlsruhe, Germany
Brij 35	Carl Roth, Karlsruhe, Germany
Bufuralol Hyrochlorid	Toronto Research Chemicals, Toronto, Canada
Bupropion Hydrochlorid	Toronto Research Chemicals, Toronto, Canada
Calcein AM	Sigma Aldrich Chemie, Steinheim, Germany
Chloroform	Carl Roth, Karlsruhe, Germany
Chlorzoxazone	Carl Roth, Karlsruhe, Germany
Coumarin crystallin	Toronto Research Chemicals, Toronto, Canada
D-(+)-Glucose	Sigma Aldrich Chemie, Steinheim, Germany
Dibenzylfluoresceine (DBF)	Carl Roth, Karlsruhe, Germany

Diclofenac	Toronto Research Chemicals, Toronto, Canada
Dicumarol (3,3 methylene-bis (4-hydroxycoumarin))	Sigma Aldrich Chemie, Steinheim, Germany
Diethylpyrocarbonate (DEPC)	VWR, Leuven, Belgium
Dimethylsulfoxid (DMSO)	Carl Roth., Karlsruhe, Germany
DMEM without Phenol Red	PAA Lab., Traun, Österreich
dNTP Mix for PCR	Axon Labortechnik GmbH, Kaiserslautern, Germany
Dulbecco's modified eagle's medium (DMEM) 10x	Biochrome, Berlin, Germany
Dulbecco's modified eagle's medium (DMEM) High glucose	Sigma Aldrich Chemie, Steinheim, Germany
Dulbecco's Phosphate buffered saline	Sigma Aldrich Chemie, Steinheim, Germany
Dulbecco's Phosphate buffered saline 10x	Sigma Aldrich Chemie, Steinheim, Germany
Essigsäure	Carl Roth, Karlsruhe, Germany
Ethanol	Carl Roth, Karlsruhe, Germany
Ethanol 99%	Carl Roth, Karlsruhe, Germany
FCS	Gibco, Paisley, UK
Fluoresceine	Sigma Aldrich Chemie, Steinheim, Germany
Glycerol	Carl Roth, Karlsruhe, Germany
Hoechst 33342	Sigma Aldrich Chemie, Steinheim, Germany
Isopropanol	VWR, Leuven, Belgium
Magnesium chloride ($MgCl_2$)	Carl Roth, Karlsruhe, Germany
Monochlorobimane (MCB)	Sigma Aldrich Chemie, Steinheim, Germany
N-(1-naphthyl) ethylenediamine dihydrochloride	Sigma Aldrich Chemie, Steinheim, Germany
O-Phtalaldehyde	Sigma Aldrich Chemie, Steinheim, Germany
Ornithine	Sigma Aldrich Chemie, Steinheim, Germany
Penicillin / Streptomycine (P/S)	PAA Lab., Traun, Austria
peqGOLD TriFast	Peqlab Biosystems, Erlangen, Germany
Phenacetin	PAA Lab., Traun, Austria
Phosphate buffered Saline (PBS)	PAA Lab., Traun, Austria
Probenecid	Sigma Aldrich Chemie, Steinheim, Germany
Reaction Buffer B for PCR	Axon Labortechnik GmbH, Kaiserslautern, Germany
Resazurin Sodium Salt	Sigma Aldrich Chemie, Steinheim, Germany
Rhodamine 123	Sigma Aldrich Chemie, Steinheim, Germany
S-Mephenytoin	Toronto Research Chemicals, Toronto, Canada
Salicylamid	Sigma Aldrich Chemie, Steinheim, Germany
Sodium hydroxide (NaOH)	Carl Roth, Karlsruhe, Germany
Sodium Pyruvate	Sigma Aldrich Chemie, Steinheim, Germany
Sulforhodamine B (SRB) sodium salt	Sigma Aldrich Chemie, Steinheim, Germany
Sulfuric acid (H_2SO_4)	Carl Roth, Karlsruhe, Germany
Taq Polymerase	Axon Labortechnik GmbH, Kaiserslautern, Germany
Tris(hydroxymethyl)-aminomethan (TRIS)	Sigma Aldrich Chemie, Steinheim, Germany
Trypan blue 0,5%	Carl Roth, Karlsruhe, Germany
Trypsin/Ethylenediaminetetraacetic acid (EDTA)	Sigma Aldrich Chemie, Steinheim, Germany
7-Hydroxycoumarin (Umbelliferon)	Carl Roth, Karlsruhe, Germany
Urea	Carl Roth, Karlsruhe, Germany

Table 2: List of Chemicals

2.1.3 Equipment

Centrifuge Fresco 17 & 21	Heraeus Instruments, Waltham, USA
Centrifuge Megafuge 40 R	Thermo Fisher Scientific, Waltham, USA
Fluorescence Microscope EVOS-fl	Peqlab Biosystems, Erlangen, Germany
FLUOstar Omega	BMG Labtech, Ortenberg, Germany
Forma 900 -80 °C Freezer	Thermo Fisher Scientific, Waltham, USA
Heratherm Oven	Thermo Fisher Scientific, Waltham, USA
Incubator BINDER	Binder, Tuttlingen, Germany
Lambda Plus Multi Channel Pipette 50 - 200 µL	Corning, Corning, USA
Lambda Plus Pipette 0.5 - 10 µL	Corning, Corning, USA
Lambda Plus Pipette 10 - 100 µL	Corning, Corning, USA
Lambda Plus Pipette 100 - 1000 µL	Corning, Corning, USA
Lambda Plus Pipette 2 - 20 µL	Corning, Corning, USA
Laminar Flow Bench Safe 2020	Thermo Fisher Scientific, Waltham, USA
Light Microscope Primo Vert	Carl Zeiss MicroImaging, Munich, Germany
LVIS Plate	BMG Labtech, Ortenberg, Germany
Magnetic stirrer RH B 2	IKA - Werke, Staufen, Germany
SecuFlow fume hood	Walder Laboreinrichtungen, Wangen, Germany
Waterbath Aqualine AL25	Lauda Dr. R. Wobser, Königshofen. Germany
Weighing scale ABJ 120-4 M	Kern & Sohn, Balingen, Germany
Weighing scale PCB 250-3	Kern & Sohn, Balingen, Germany
Intas GelDoc	Intas Science Imaging, Göttingen, Germany

Table 3: List of Equipment

2.1.4 Programs

OMEGA Software for FluoStar,	BMG Labtech, Offenburg, Germany
ImageJ V1.53	National Institute of Health, Maryland, USA
GraphPad V5.01	Graph Pad Software, San Diego, USA
Word	Microsoft
Excel	Microsoft
Intas GelDoc	Intas Science Imaging, Göttingen, Germany
Endnote V9.2	Clarivate Analytics

Table 4: List of Programs

2.1.5 Kits used

ThermoFisher First Strand cDNA Kit	Thermo Fisher Scientific, Waltham, USA

Table 5: List of ready kits used

2.2 Methods

2.2.1 Cell culture

The HepG2 cells were cultured in 175 cm^2 flasks before experimentation. For experiments, the cells were cultured in either 2D, sandwich or scaffold culture in 24-well-plates. Medium consisted of Dulbecco's Modified Eagle's Medium with high glucose, to which 1% Penicillin/Streptomycin (P/S) and 10% Fetal Calf Serum (FCS) were added. Cell culture flasks and plates were placed in an incubator at 37 °C, 5% CO_2. The medium in the cell culture flasks was exchanged every 3-4 days.

2.2.1.1 Trypsination and splitting

Upon reaching 80-90% confluency, as assessed under the microscope, the cells were washed with Dulbecco's Phosphate Buffered Saline (DPBS). Then, 1,5-2 ml of Trypsin/EDTA (T/E) were added for a 175 ml flask. They were placed in the incubator at 37 °C, 5% CO_2 and after 10 minutes it was assessed whether all cells had been mobilized from the surface. When all cells were in suspension, 10 ml of medium with FCS were added to dilute and inactivate the T/E and the solution was transferred into a 50 ml falcon tube, in which it was centrifuged at 600 *g for 10 minutes. The supernatant was discarded, and the pellet resuspended, either to be used in experiments or transferred back into a cell culture flask. For experiments, the cells were counted in a Neubauer cell counting chamber using Trypan blue as a dye and diluted to the necessary concentrations.

2.2.1.2 Stimulation with 5-AZA and Vitamin C

After 24 hours of incubation to allow for cell adherence, half of the cells were treated with medium containing 10 µM 5-Azacytidine (5-Aza) and 0.5 mM Vitamin C as well as 10% FCS and 1% P/S. The cell solution was renewed after 24 hours to maintain a steady concentration. The protocol was adapted after the protocols for HLE, and Huh-7 cell lines of Sajadian *et al.* (Sajadian *et al.*, 2016).

2.2.2 Sandwich culture

2.2.2.1 Isolation of rat tail collagen

For the sandwich cultures and the cryogels, collagen was isolated from rat tail tendons. For this, the tails were broken between the vertebrae and the tendons pulled out. The tendons were then air-dried in the cell culture bench under ultraviolet light for sterilization

for 24 hours. After this, 3.5 g of the isolated tendons were stirred in 1 l of 0,1% acetic acid for the cryogels. For the sandwiches, 8.4 g of the isolated tendons were stirred in 1 l of 1% acetic acid for 48 hours.

2.2.2.2 Preparation of Sandwich culture

The preparation of a sandwich culture was modified after Dunn *et al.* (Dunn *et al.*, 1989). To prepare the collagen solution, one part of 10x Dulbecco's Modified Eagle's Medium (DMEM) with Phenol Red was mixed with nine parts of the rat tail collagen (8,4 g/l). This solution was then neutralized stepwise to pH 7,3 using Sodium Hydroxide (NaOH) and repeatedly agitated. To avoid polymerization and contamination, all of the steps were performed on ice and under the laminar flow bench. When neutralized, 50 µl of the solution were spread in each of the wells of a 24-well-plate. The plates were then placed in the incubator for 30 minutes to polymerize, after which cells were seeded on them. After 4 hours of cell attachment a second layer of collagen solution was added on top of them and after further 30 minutes for polymerization, medium was added.

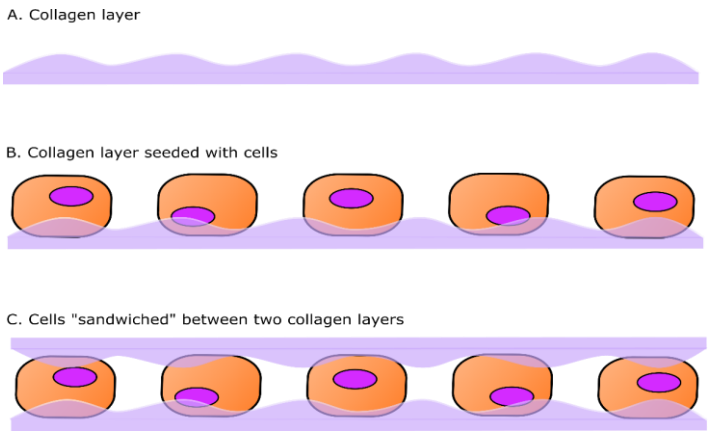

Figure 4: Preparation of sandwich culture. After preparing the surface of the cell culture plate with collagen, cells are added, left to adhere, and then coated with another layer of collagen

2.2.3 Preparation of cryogels

2.2.3.1 Creation of scaffolds

A protocol similar to that used by Ruoß *et al.* for the creation of cryogels from a rapidly polymerizing solution was used (Ruoß *et al.*, 2018). Figure 5 shows the scaffold creation process. For standardized casting forms, we used 2 ml syringes with a diameter of 9,82 mm, from which we removed the tips. Because the solution rapidly polymerizes after all

the components have been added, it is important to work on ice and to make sure all the necessary chemicals and equipment are ready and cooled before starting. In the first step, ddH_20, rat tail collagen and cold fish gelatin were mixed in a 50 ml falcon and thoroughly agitated. Then poly (2-Hydroxyethyl methacrylate) (pHEMA) and bis-acrylamide (BAA) were added, working under the fume hood. The solution was then agitated again. All these steps were performed while keeping the components on ice.

In the final step, tetramethylethylendiamine (TEMED), ammonium persulfate (APS) and glutaraldehyde (GA) were added in quick succession and the solution was briefly agitated. It was then immediately poured into the prepared syringes and placed at -20 °C for 24 hours. Table 6 shows the different scaffold compositions used for experimentation.

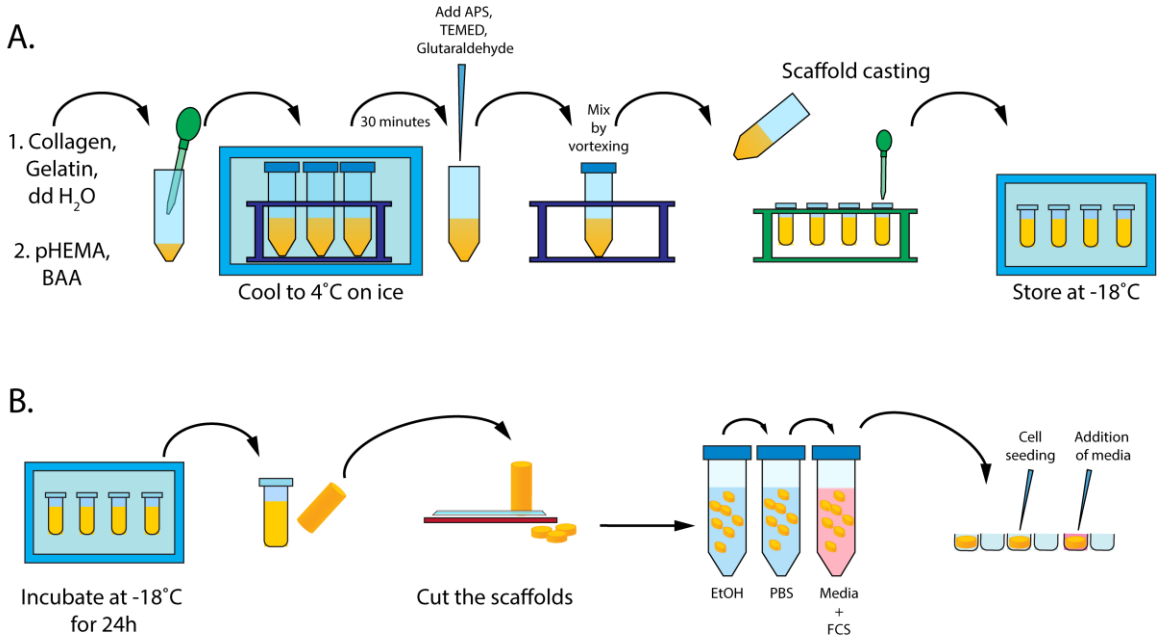

Figure 5: Scaffold creation (modified after Ruoß et al. *((Ruoß* et al., *2018)). Briefly, the polymerization solution is cooled, the cross-linkers are added, after which they are quickly mixed and poured into the casts. While Polymerization takes place, they are stored at -18°C. After Polymerization is completed, they are removed from the casts, cut, sterilized, washed with DPBS and incubated in medium before being used in cell culture.*

Substance	Composition 1	Composition 2	Composition 3	Composition 4
pHEMA 98%	1,0 ml	1,6 ml	2,0 ml	3,0 ml
BAA 2%	500 µl	260 µl	1,0 ml	1,5 ml
Collagen 3,5 g/l	1,0 ml	3,0 ml	1,0 ml	1,0 ml
Gelatin 300 g/l	2,0 ml	-	2,0 ml	2,0 ml
ddH_2O	5,5 ml	5,14 ml	4,0 ml	2,5 ml

Table 6: Table of scaffold compositions and the concentration of contents

2.2.3.2 Cutting and sterilization of scaffolds

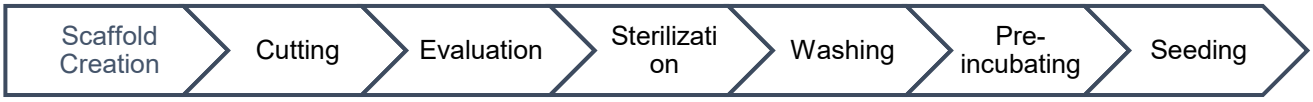

Figure 6: Scaffold creation workflow

Figure 6 shows the scaffold creation workflow. After 24 hours of polymerization, the syringes were taken out of the freezer and the polymerized solution was cut into 3 mm thick disks. The top and bottom 6 mm as well as any unevenly cut scaffolds were discarded. The scaffolds were then viewed under the fluorescence microscope, where they could be evaluated regarding regular pore formation without the need for a dye due to the innate fluorescence of the polymerized proteins.

The scaffolds were then placed in a 50 ml falcon tube and suspended in 70% ethanol (without additives) and placed on the orbital shaker for 6-24 hours for sterilization. After sterilization, they were repeatedly washed with DPBS to remove the ethanol. Before seeding could be performed, the scaffolds were placed in cell culture plate wells and submerged in DMEM with 10% FCS and 1% P/S and placed in the incubator overnight to allow for the medium to diffuse into the scaffold. Preliminary tests showed that without medium incubation the adherence and survival of cells were severely limited. The protocol was adapted accordingly with the scaffolds being pre-incubated for 24 hours before seeding of cells.

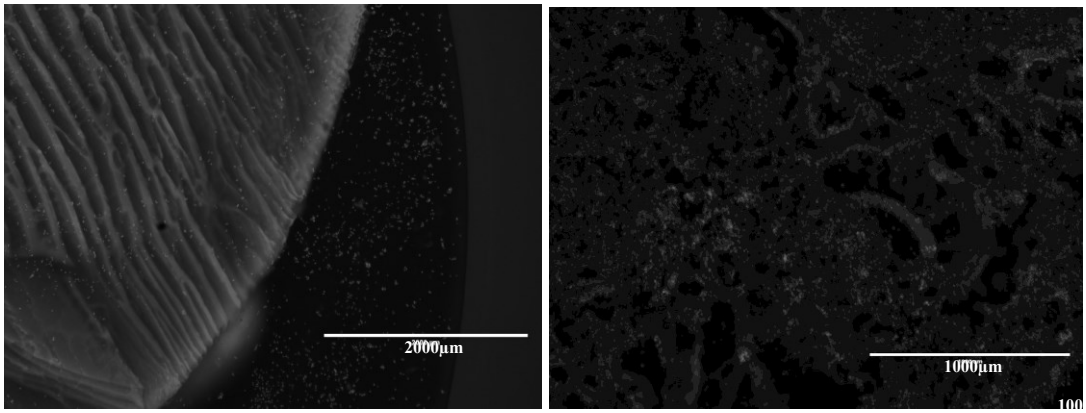

Figure 7: Scaffolds and adherent cells without (left) and with (right) 24 hours of pre-incubation in medium with FBS

2.2.3.3 Seeding of cells on scaffolds

On day 0, cells were seeded on either scaffold, sandwich or in 2D culture. After seeding was complete according to the individual protocol, they were placed in the incubator for

24 hours with medium to allow for cell adherence. For experiments, HepG2 cells in passage 8 to 10 were used, as it has been demonstrated that between passage 8 and 16 enzyme activity is the most stable (Lin *et al.*, 2012; Westerink *et al.*, 2007).

2.2.3.3.1 Surface seeding

On the day the cells were seeded, the medium was removed from the scaffolds and then air-dried for 30 minutes to allow for better absorption of the cell solution. After this, 50 µl of cell solution (concentration 2x 10^7 cells/ml) were added on top of the scaffold. The scaffolds were incubated at 37 °C, 5% CO_2 for 4 hours to allow for cell adherence and then covered in medium.

2.2.3.3.2 Orbital seeding

For orbital seeding, the scaffolds were placed in a sterile falcon tube and submerged in medium containing 1-3 x 10^6 cells/ml. Cells were then placed on the orbital shaker for 30 - 60 minutes at 2-5 rotations/minute to allow flowing of the medium through the cryogels. Afterwards, they were placed in a sterile 24-well-plate and placed in the incubator for 4 hours to allow for adherence. They were then covered in medium.

2.2.4 Microscopy

Cells and scaffolds were placed under a microscope for evaluation of morphology, viability, and confluence. The cells could be evaluated using either normal light for morphology or staining with Hoechst and Calcein AM. The structure of the scaffolds could be assessed using the innate fluorescence of its protein bonds, which could be increased by dyeing it with Hoechst, Calcein AM or Sulforhodamine B (SRB). Before staining, the medium was removed from the cells, and they were washed three times with DPBS.

2.2.4.1 Pore diameter measurement

All conditions showed formation of pores in at least a portion of the scaffold. For each condition, a total of three pictures was analyzed with 30 pores measured for each picture. Formations of long “channel”-like pore structures were not analysed in this fashion to avoid skewing the measurements (Kumari *et al.,* 2016).

2.2.4.2 Hoechst staining

Hoechst is a dye that interacts with a cell's DNA and therefore stains the nuclei of both living and dead cells. The stock solution of 1 mg/ml was diluted 1:1000 in DPBS and then transferred into the wells. They were then incubated for 30 minutes at 37 °C, 5% CO_2 and washed four times with DPBS. Microscopy was then performed in the DAPI channel with excitation at λ= 358 nm and emission at λ= 461 nm, the reported wavelengths for this dye (Romano *et al.*, 2018, Atale *et al.*, 2014).

2.2.4.3 Calcein AM Staining

Calcein acetoxymethyl ester (Calcein AM) is a dye that can only be transported through the cell membrane by active transport and therefore only accumulates in living cells. The 1:1000 diluted stock solution (which was 4 mM) was transferred onto the cells and incubated for 30 minutes. They were then washed four times with DPBS and placed under the microscope in the GFP channel (excitation λ= 488 nm, emission maximum λ= 510 nm) (Wang *et al.*, 2008).

2.2.4.4 SRB Staining

Sulforhodamine B (SRB) is commonly used to quantify cells in 2D culture. It binds to proteins under acidic conditions. For evaluation of scaffolds, they were submerged in a 0.4% solution of SRB in 1% acetic acid for 1 minute. They were then washed five times in 1% acetic acid and placed under the microscope, where they were assessed using the RFP channel (Excitation λ= 558 nm, emission maximum λ= 583 nm). Cells were first fixed with ethanol and then stained as described above (Skehan *et al.*, 1990).

2.2.5 Functional assays

After seeding cells out on day 0, they were stimulated for 48 hours and then on day 3 the metabolic experiments were started. In 2D and sandwich culture, 200,000 cells in 700 µl medium were used in 24-well-plates (1,9 cm^2 per well). For scaffold culture, 200,000 cells were used per scaffold.

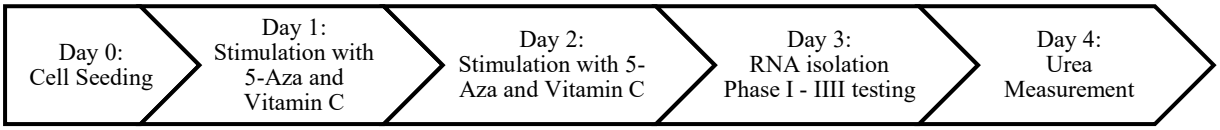

Figure 8: Workflow of the Stimulation and Testing

2.2.5.1 Ammonia detoxification

For the measurement of Urea production, the cells were washed three times with DPBS. Then the cells were incubated for 24 hours with reaction solutions containing magnesium chloride ($MgCl_2$), sodium pyruvate, ammonium chloride (NH_4Cl) and L-ornithine in DPBS.

	U1	U2	U3
$MgCl_2$	1 mM	1 mM	1 mM
Sodium pyruvate	1 mM	1 mM	1 mM
NH_4Cl	-	300 mM	300 mM
L-ornithine	-	-	100 mM

Table 7: Contents of Ammonia detoxification test solutions

After 24 hours, 80 µl of the supernatant were transferred into a 96-well-plate. To this, 60 µl of O-Phtaldehyde solution (0.75 M sulfuric acid (H_2SO_4), 15 mM O-Phtalaldehyde, 4 mM Brij-35) and 60 µl of NED-reagent (2.25 M H_2SO_4, 80 mM Boric acid, 3 mM N-(1-naphthyl) ethylenediamine dihydrochloride (NED), 4 mM Brij-35) were added and incubated for 2 hours. For each measurement, a standard curve containing concentrations of Urea ranging from 0 µg/ml to 100 µg/ml was incubated in triplicate.
After the incubation, the absorption at λ= 460 nm was measured in the plate reader and the values were normalized using the standard curve (Jung *et al.*, 1975; Zawada *et al.*, 2009).

2.2.5.2 CYP activity assays

For the measurement of the activity of CYP1A2, CYP2C9 and CYP3A4 the cells were prepared by removing medium and washing with DPBS twice on day 3. A test solution

containing an enzyme reactant, medium and inhibitors of the respective phase II enzymes was prepared. Then the test solution was added to the wells and incubated at 37 °C, 5 % CO_2 for 30 minutes. After 30 minutes, 100 µl of supernatant were transferred to a 96-well plate. Alongside the supernatant, a dilution curve of the respective transformation product was pipetted into the 96-well plate. The plate was then analyzed using the plate reader (Donato *et al.*, 2004). Table 8 contains reagents and the wavelengths from the plate reader at which measurements were taken.

	CYP 1A2	CYP 2C9	CYP 3A4
Reactant	7-Ethoxycoumarin 25 µM	Dibenzylfluoresceine 20 µM	7-Benzyloxy-4-coumarin 10 µM
Product	7-Hydroxycoumarin	Fluoresceine	7-Hydroxy-4-coumarin
Phase II Inhibition	Salicylamid 1µM Probenecid 2 µM	Dicoumarol 10 µM	Salicylamid 1.5 µM Probenecid 2 µM
Excitation / Emission	355 nm / 460 nm	485 nm / 520 nm	355 nm / 520 nm
Standard curve	7-Hydroxycoumarin 1 pmol/µl	Fluoresceine 5 mM	7-Hydroxy-4-coumarin 50 mM

Table 8: Contents of CYP test solution

2.2.5.3 Phase II measurement

2.2.5.3.1 Uridine diphosphate glucoronosyltransferase (UGT) measurement

For the activity of UGT, the ability of the cells to conjugate 4-Methylumbelliferone (4-MU) with glucose from Uridine diphosphate (UDP)-Glucose was measured. After 48 hours of stimulation, the cells were washed twice with DPBS. Then, 700 µl of a 6.25 µM 4-MU solution in serum-free medium were added to the wells and incubated for 30 minutes and 60 minutes respectively. After incubation, 100 µl of the supernatant were transferred to a 96-well plate and measured in the plate reader at excitation 355 nm and emission 460 nm. It was compared to a standard curve of 4-MU with the highest concentration at 6.25 µM. It is important to note that in this reaction, the emission of the unconjugated 4-MU is measured, so a decrease in emission is due to conjugation from increased enzyme activity (Donato *et al.*, 2004).

2.2.5.3.2 Glutathione S-transferase (GST) activity measurement

GST conjugates monochlorobimane (MCB) with free glutathione. After removing the medium and washing the cells with DPBS, 700 µl of an 80 µm solution of MCB in serum-free medium was added. The cells were then incubated for 30 minutes, after which 100 µl of the supernatant were transferred to a 96-well-plate. Fluorescence was then measured at emission λ= 355 nm and excitation λ= 460 nm. For this experiment normalization was done in relation to cell number (Donato *et al.*, 2004).

2.2.5.4 Efflux assays

The membrane-bound enzymes MDR1 and MRP1 transport molecules across the cell membrane. The cells were washed three times with DPBS, then a solution of either 4 µM 5(6)-Carboxy-2',7'-dichlorofluorescein diacetate (5-CDFA) for MRP1 or 3 µM rhodamine (for MDR1), both in DPBS, was added and left to incubate for 30 minutes. During this time, the cells took up the compounds by passive diffusion. After 30 minutes, the solutions were removed, and the wells washed with DPBS another three times. Then a 11 mM glucose solution of DPBS was added for 30 minutes, after which the supernatant was collected and measured in the plate reader at excitation λ= 485 nm and emission λ= 520 nm for both. The results were compared to a standard curve of 5-Carboxyfluorescein (5-CF) and rhodamine, respectively (Schyschka *et al.*, 2013).

2.2.6 Resazurin conversion assay

Due to the high protein content of the scaffold, SRB staining, a well-established method of cell quantification could not be used. Instead, a resazurin assay can be used to quantify cells in 3D- or extracellular matrix environments (Uzarski *et al.*, 2017). 2D and sandwich culture cell quantification was also performed using resazurin conversion to avoid creating additional confounding factors. Standard curves were created in 2D culture (Figure 9).

The conversion of resazurin to resorufin is an assay that can be used to determine cell number in cell culture. Viable cells have the ability to convert the redox dye resazurin into resorufin, for which the fluorescence can be measured at 590 nm. For the conversion assay, the cells were washed with DPBS once for 2D culture and twice for sandwich and scaffold culture to remove any interfering substances. 0.7 ml of a 0,0025% resazurin in DMEM solution was then added to the wells and incubated at 37 °C for 60 minutes in 2D

and sandwich culture and 150 minutes for the cryogels. After incubation, 100 µl of the supernatant was pipetted into a 96-well-plate. Fluorescence was then measured at an excitation wavelength of λ= 544 nm and emission wavelength of λ=590-10 nm using an Omega Plate Reader (Ruoß *et al.*, 2018). For normalization of background values, the background measurements in wells without cells for 2D, sandwich and cryogel culture was determined separately from each other.

For normalization, two standard curves were created (Figure 9). For the 2D and sandwich wells, a standard curve with an incubation time of 60 minutes was created. As preliminary experiments had shown much lower cell numbers in 3D culture, a separate standard curve was created for 3D culture wells. Accordingly, in experiments that required normalization to cell number, the wells were incubated for the corresponding time.

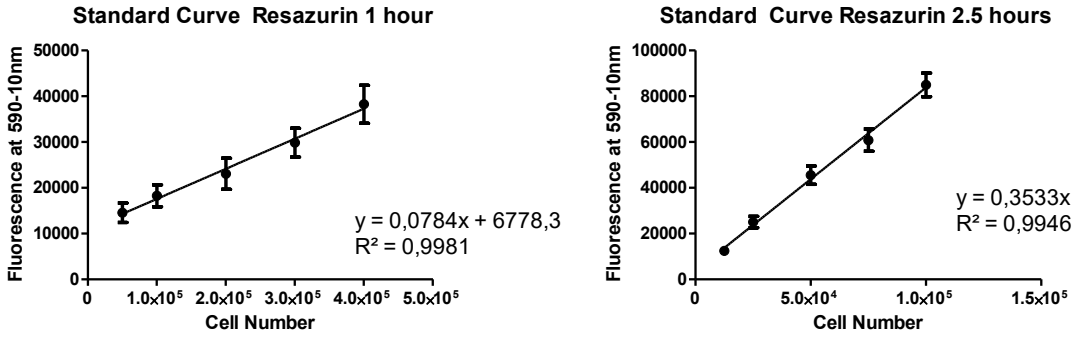

Figure 9: Standard curves of Resazurin conversion after 60 and 150 minutes of incubation. For each standard curve, cells were cultured in 2D with N ≥3 and n≥15 and conversion was measured after 1 and 2.5 hours respectively. The standard curve was created using linear regression

2.2.7 RNA isolation

RNA isolation was performed in 2D, sandwich and scaffold culture after 48 hours of stimulation with 5-Aza and Vitamin C as described above. The wells were washed twice with DPBS. In 2D culture the cell detergent TriFast was added to the cell culture plates and the wells were thoroughly scraped using a scraper.

For cells in sandwich culture, the bottoms of the wells were covered in a solution containing collagenase and incubated at 37 °C for 30 minutes. Afterwards, the bottom of the well was covered with TriFast well and the cells were recovered using a cell scraper and briefly centrifuged and the phase containing the cells recovered. For scaffold culture, the scaffolds were taken out of their wells and shock-frozen with liquid nitrogen. While frozen, the scaffolds were crushed in a grinder and then covered with TriFast. The mix

was then stirred and afterwards filtered through a fine cloth to remove any pieces of scaffold remaining. After the cells had been suspended in TriFast, 100 µl of chloroform was added per 500 µl of TriFast and carefully mixed. Afterwards the samples were centrifuged at 14,000 *g for 10 minutes at 4 °C. The clear phase containing the RNA was then transferred to a fresh Eppendorf tube containing isopropanol. After carefully mixing the samples again, they were then centrifuged at 14,000 *g, 4 °C for 10 minutes again and the supernatant removed and replaced by 70% ethanol. This step was repeated once and then the samples were resuspended in diethyl carbonate water (DEPC H_2O) (Sambrook *et al.*, 1989).

2.2.7.1 cDNA synthesis

In the complementary DNA (cDNA) synthesis step, the entirety of the mRNA in each sample is transcribed into DNA. This allows polymerase chain reaction (PCR) to be performed, as primers used can only bind to DNA. For this step, the RNA samples were mixed with a ready mix containing a surplus of nucleotides, random primers, and reverse transcriptase, which is needed for transcribing RNA into DNA. The DNA FirstStrand kit from ThermoFisher was used and the samples were incubated in the Thermocycler according to the manufacturer's instructions (Thermo Fisher Scientific, 2017).

2.2.8 PCR

Polymerase Chain Reaction (PCR) is a process in which a certain gene, for which the primer sequence is known, is amplified using a heat-stable polymerase. It can be used to detect the level of gene expression in each sample for comparison. Each value is normalized using the expression of the house-keeping gene Hypoxanthin guanine phosphoribosyl transferase (HPRT), that are stably expressed under different conditions. For PCR, the samples were mixed with a mastermix containing KAPA2G-polymerase, nucleotides and the specific primers and incubated in the Thermocycler (Biosystems, 2017).

2.2.9 Gel electrophoresis

A gel with 1.5 g agarose dissolved in 100 ml of ddH_2O and 7 µl ethidium bromide per was poured and left to harden for 30 minutes. Afterwards, the expanded cDNA samples were loaded into the pockets and an electrical current of 90 V was applied for 40 minutes. Images were then made using the Intas GelDoc system. The images were analyzed using

ImageJ. Values were normalized against the Hypoxanthin guanine phosphoribosyl transferase (HPRT) expression of the respective samples (Sambrook *et al.*, 1989).

2.3 Statistical analysis

Consultation for the statistical analysis and study design was held with the 'Institut für Klinische Epidemiologie und angewandte Biometrie of the Universität Tübingen'.
Statistical analysis of all experiments was done using SPSS Version 28.0.0.0 by IBM. Normalization was done in relation to cell number, determined by resazurin conversion. To determine whether the data sets follow a normal distribution, D'Agostino-Pearson test was performed. As natural distribution could not be assumed for the data sets, a non-parametric test was chosen to test for significant differences. Grubb's test was performed to test for outliers in the data sets.
Kruskal Wallis test was chosen, as all the assumptions for performing the test were met by the data; An independent variable with more than two groups (in this case six) as well as one dependent variable on an ordinal scale, for which normal distribution could not be determined using the D'Agostino-Pearson test. For the comparisons, in which the null hypothesis (H_0: measurement medians are equal) could be rejected, a Dunn's multiple Comparison's test was done afterwards to determine, which of the groups varied. For pairwise comparison, a Mann-Whitney-U-test was performed.
Statistical tests were performed two-sided as an exploratory data analysis using $p < 0.05$ (*), $p < 0.01$ (**), and $p < 0.001$ (***) as level of significance as marked in the graphs.
Gel electrophoresis images were analyzed using the open-source ImageJ version 1.53. Data was normalized in relation to the housekeeping gene GAP-DH. Bar graphs were created using GraphPad Prism Version 5.

3 Results

3.1 Scaffold optimization / characterization

3.1.1 Scaffold composition

The scaffolds were prepared according to a protocol as described above. The goal was to find a composition of the different substrates that allows for reproducibility, ease of handling and mechanical stability as well as an optimal pore structure. Several promising compositions from unpublished previous experiments were picked out and investigated further. The detailled compositions can be found in Table 6: Table of scaffold compositions and the concentration of contents.

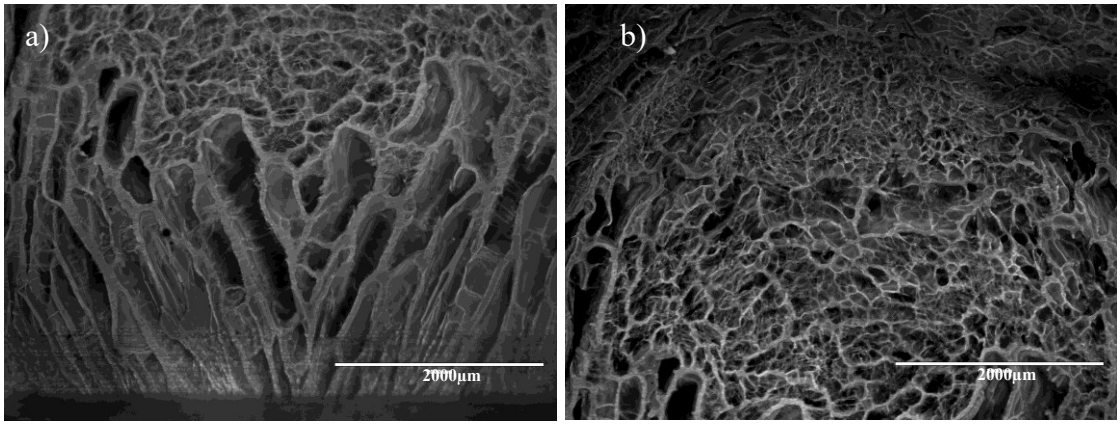

Figure 10: Microscopy of the top of scaffolds from composition 1 (scalebar is 2000 µm)

The scaffolds of composition 1, which had the lowest pHEMA concentration, as well as the lowest protein concentration overall, showed the formation of a network of pores over most of the surface (Figure 10b). On the sides of the scaffold, where it had been closest to the syringe wall, there was formation of long vertical pore “tubes”, several mm in length. These tubes could be found in the outermost 1-2 mm of the scaffold (Figure 10a). Of the scaffold compositions tested, composition 1 showed the least batch-to-batch variation in pore structure.

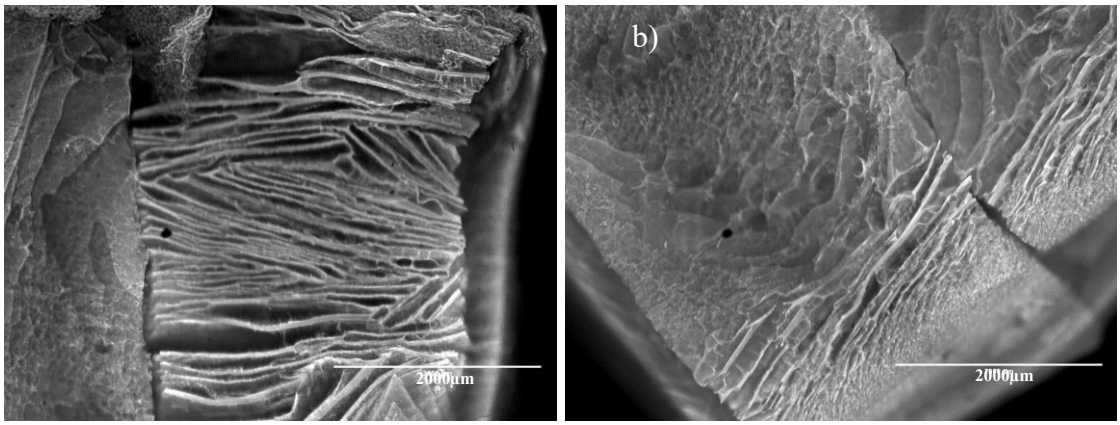

Figure 11: Microscopy of cross-sections of scaffolds from composition 2 (scalebar is 2000 µm)

In composition 2, which utilized a higher collagen concentration than any of the other compositions tested, but no gelatin, most of the scaffold matrix was made up of long vertical pore "tubes", similar to those found in the scaffolds from composition 1. These tubes could be found across the entire diameter of the scaffold as shown in Figure 11a). On a small subsection of scaffolds produced from composition 2, the formation of smaller, networked pores could be observed toward the center of the scaffold (Figure 11b).

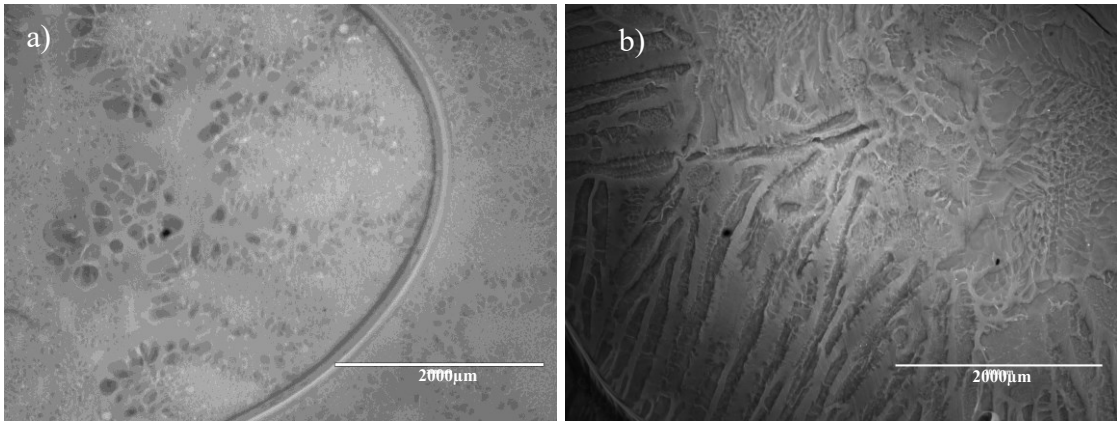

Figure 12: Microscopy of the top of scaffolds from composition 3 (scalebar is 2000 µm)

In the scaffolds created from composition 3, the formation of both networked small pores as well as tubular pores could be seen (Figure 12b). In addition, due to the high protein content, a number of larger pores that appeared to be entirely encumbered by scaffold material could be seen, especially toward the center of the scaffold (Figure 12a).

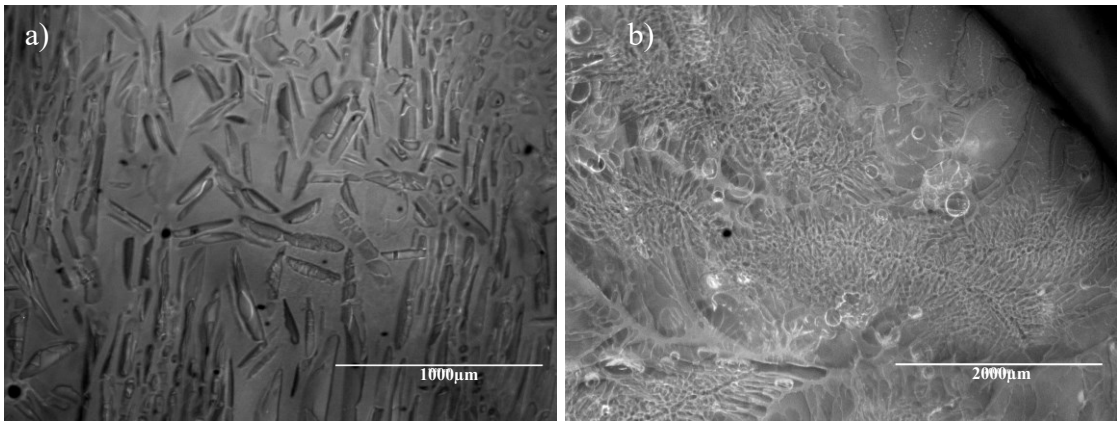

Figure 13: Microscopy of the top of scaffolds from composition 4 (scalebar on the left is 1000 µm, on the right 2000 µm)

In the scaffolds created from composition 4, the composition with the highest pHEMA concentration, the center pores appeared to be encumbered by thick walls of scaffold matrix (Figure 13a). As in the other compositions tubular pores could be seen on the peripheral portions of the scaffold and a network of small pores could be seen in between (Figure 13b).

3.1.2 Pore size measurements

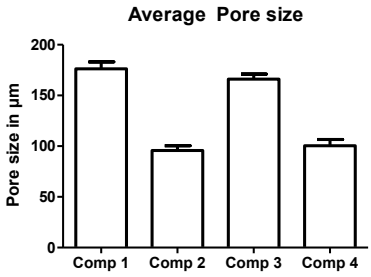

	Average	Range
Composition 1	176,3 µm	67,1 - 358,6 µm
Composition 2	95,7 µm	37,3 – 357,2 µm
Composition 3	166,1 µm	66,7 – 272,9 µm
Composition 4	100,4 µm	24,8 – 364 µm

Figure 14: Pore size measurement of scaffolds from composition 1-4. For each composition, 30 pores were measured from an area of uniform pore formation

Composition 1, which had the lowest protein content, also showed the largest pores of the compositions investigated. Accordingly, the compositions with the highest protein concentrations comp. 2 and comp. 4 showed much smaller pores on average.

The average pore size described for the scaffold compositions investigated, which ranges between 97,7 µm and 176,3 µm, is several times larger than the pore size of decellularized liver, which is around 22.02 ± 0.65 µm (Mattei, *et al.*, 2018). We deemed this acceptable, as the goal is to distribute cells among the interior of the entire scaffold, not just the outer surface.

3.1.3 Summary of the scaffold creation results

None of the scaffolds showed any macroscopic degradation when exposed to the substances required to use them in cell culture. However, the scaffold from composition 2, which was created without gelatin, was much less mechanically stable and prone to breaking apart when transferred.

The diameter of pores in and on the scaffold is an important factor in allowing cells to penetrate further into the scaffold and to provide them with nutrients and medium (Kumari *et al.*, 2016). We found that all four investigated scaffold compositions showed sufficient pore diameter to allow for nutrients and cells to pass through, with the average diameter being between 95.7 – 176.3 µm.

Interestingly, in all four investigated compositions, we found long, mostly vertical pores toward the outer edges of the scaffold. This might be caused when freezing occurs too fast during polymerization from the outside inward with large ice crystals forming within. Alternative experimental approaches include cooling all components down to 4°C before adding the polymerizing agents TEMED and APS or achieving a more stable surrounding temperature by using an ethanol bath (Teng *et al.*, 2018). In the compositions with a higher protein content of the polymerization solution, composition 3 and 4, we found much smaller pores as well as thicker pore walls. In solution 4, many pores apparently did not communicate with other pores. Composition 1 was chosen for further testing, as it was mechanically stable, had a good porosity and high reproducibility.

3.1.4 Scaffold seeding

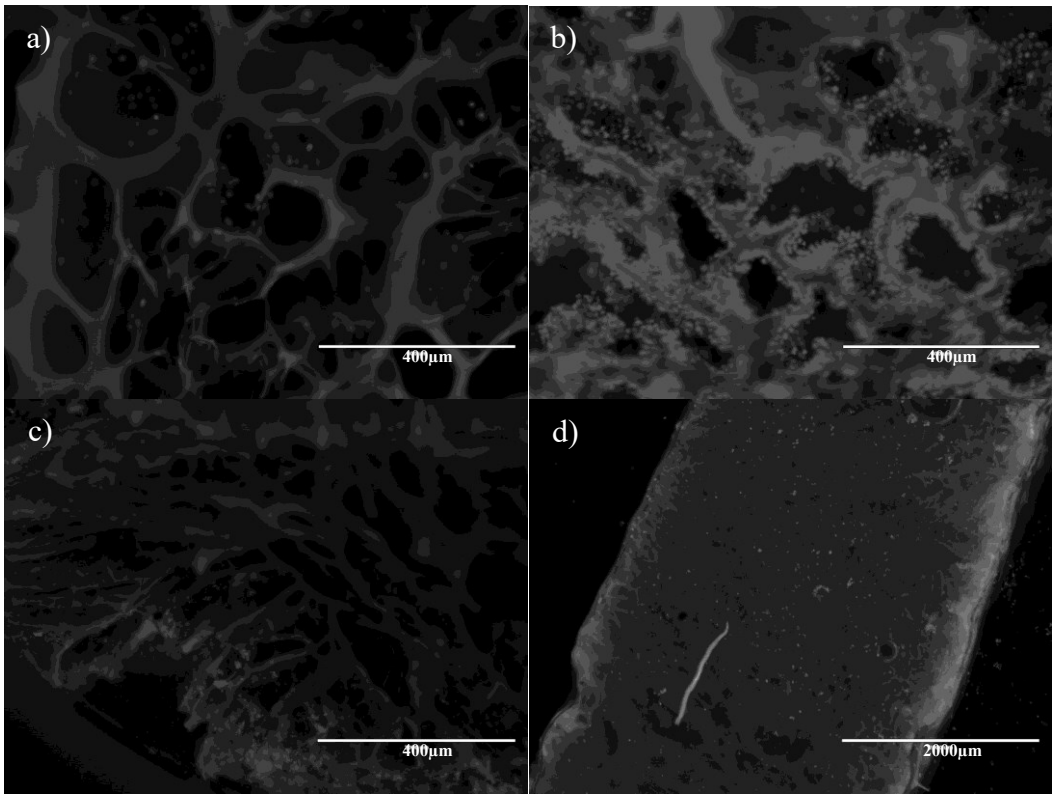

Figure 15:Microscopy of different seeding techniques: a) top-down view of orbital seeding b) top-down view of surface seeding c) cross-section of orbital seeding d) cross-section of surface seeding (seeding done to the right-facing surface of scaffold)

As the cells are supposed to not only adhere to the surface of the scaffold, but to the pore walls deep inside the scaffold as well, we investigated several methods of seeding. In surface seeding, a solution containing cells is pipetted on top of the scaffold, while in orbital seeding, the scaffold is submerged in a cell solution, which is then continuously gently agitated. Orbital seeding can potentially distribute the cells more evenly across the surface as well as deeper within the scaffold. Major drawbacks of orbital seeding include the high cell number required as well as the practical imposition of not being able to agitate the cell solution within the incubator (Melke *et al.*, 2020).

Fluorescence microscopy of scaffolds seeded with the orbital seeding method as well as with the classic surface seeding method (Figure 15) showed that in both cases cells adhered only to the surface of the scaffold and did not migrate deeper into the scaffold. Scaffolds seeded with the orbital seeding method showed that most cells adhered to the scaffold in the pores closest to the surface with few cells penetrating deeper into the scaffold. Scaffolds seeded with a surface-seeding technique also showed most cells adhering to the surface or several µm into the matrix. In surface-seeding, the density of cells, as observed using fluorescence microscopy, was much higher.

As a result, surface seeding was chosen for the experiments

3.1.5 Cell morphology

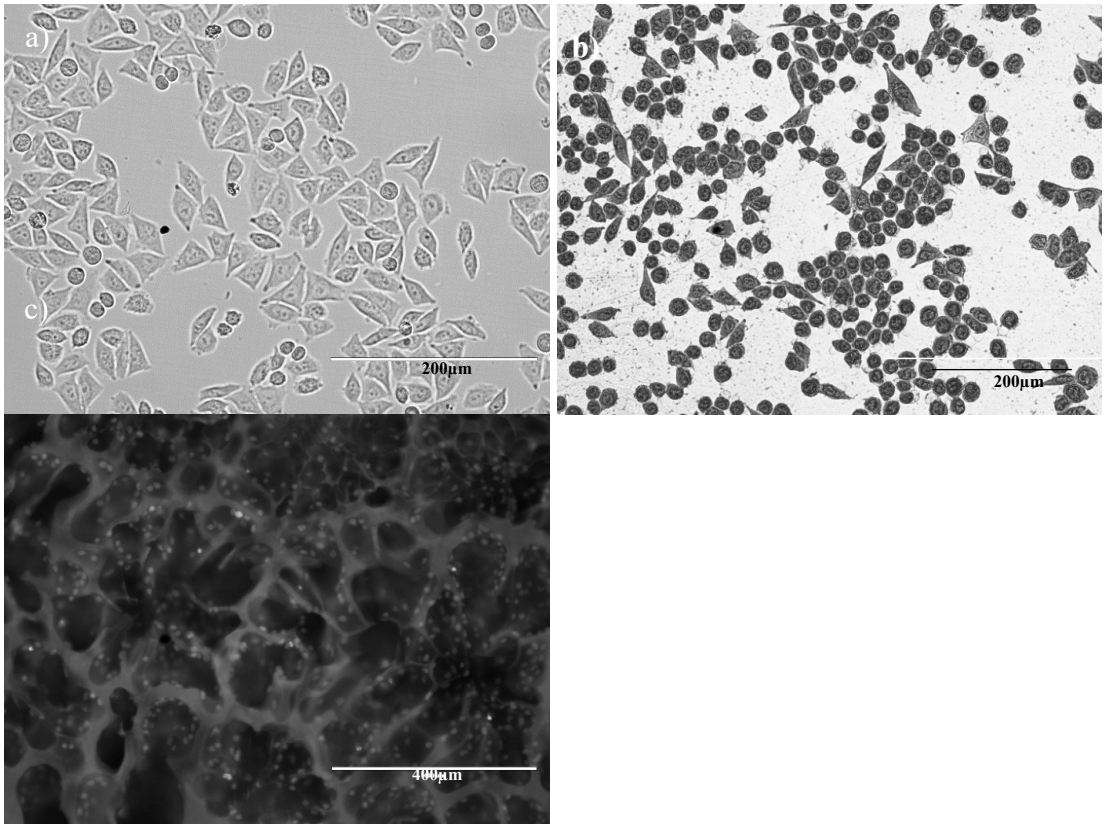

Figure 16: Cell morphology of HepG2 cells in 2D (left, sandwich culture(middle) and 3D culture. Scalebar of a) and b) is 200 µm and of c) is 400 µm

In 2D-culture (Figure 16a), HepG2 cells have a distinct triangular morphology, while in sandwich (Fig. 16b) and 3D culture (Fig 16c), the cells appear rounder. Note that the picture of the 3D culture was taken at a different magnification, due to the high level of fluorescence from the scaffold.

3.2 Functional tests

We compared the metabolic function of HepG2 cells cultured on different mechanical substrates such as 2D sandwich culture and 3D scaffold culture as well as their response to different stimulants.

Figure 17 shows the urea production over 24 hours in a basic solution containing Sodium pyruvate as an energy substrate as well as $MgCl_2$ without ammonium chloride. The lowest activity was detected in the 2D culture stimulated with 5-Aza and Vitamin C, while the highest activity was measured in 3D culture stimulated with Vitamin C. Both the AzaC and the unstimulated 3D conditions showed a significantly higher rate of urea synthesis

compared to the stimulated 2D culture. They also both showed a significantly higher rate of synthesis compared to the AzaC sandwich culture.

3.2.1 Ammonia detoxification

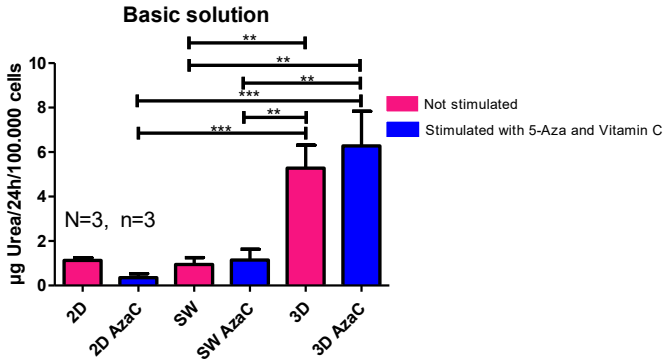

Figure 17: Urea production over 24 hours in a basic solution
Ammonia detoxification after 24 hours incubation in a basic solution by HepG2 cells in 2D, sandwich culture (SW) and on scaffolds (3D). Blue bars represent cells stimulated for 48 hours with 10 µM 5-Aza and 0.5 mM Vitamin C, while blue bars represent cells not stimulated. The ammonia detoxification was quantified by determining the urea production in 24 hours. The values were normalized to cell number determined by resazurin conversion assay. Bars represent mean ±SEM; N = 3, n = 3.

When comparing the unstimulated 2D samples with the other test conditions, we did not find a statistically significant difference. We did, however, find a statistically significant improvement of function in unstimulated 3D when compared to unstimulated sandwich culture.

For 2D, sandwich and 3D culture respectively, there was no significant difference of synthesis between AzaC and unstimulated samples of the same culture type.

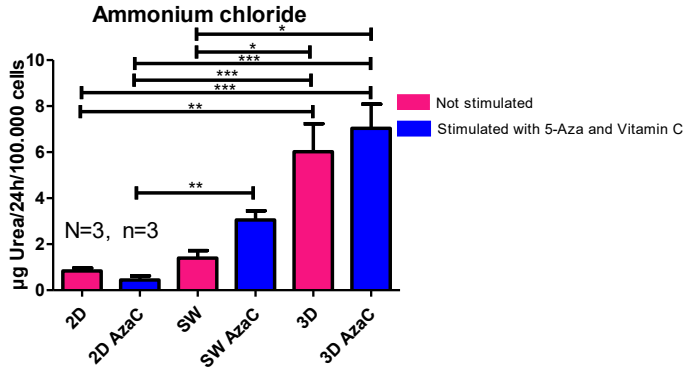

Figure 18: Urea production over 24 hours in a solution containing ammonium chloride
Ammonia detoxification after 24 hours incubation in a basic solution by HepG2 cells in 2D, sandwich culture (SW) and on scaffolds (3D). Blue bars represent cells stimulated for 48 hours with 10 µM 5-Aza and 0.5 mM Vitamin C, while blue bars represent cells not stimulated. The ammonia detoxification was quantified by determining the urea production in 24 hours. The values were normalized to cell number determined by resazurin conversion assay. Bars represent mean ± SEM; N = 3, n = 3.

Similar to the basic solution, the lowest activity in the solution containing ammonium chloride was measured in the AzaC 2D culture with the highest activity in the AzaC 3D culture, as seen in Figure 18.

We saw a statistically significant increase in activity between the 2D unstimulated group and both the AzaC and the unstimulated 3D conditions. Equally, we saw significantly higher activity in both 3D conditions when compared to the unstimulated sandwich culture.

When comparing 2D AzaC vs. unstimulated samples, no significant difference was found. Similarly, when comparing sandwich AzaC vs. unstimulated samples, no significant difference was found. In addition, comparing 3D AzaC vs. unstimulated samples, no significant difference was found. In summary, despite both the AzaC sandwich and 3D culture showing higher activity, we did not find a significant improvement in AzaC samples.

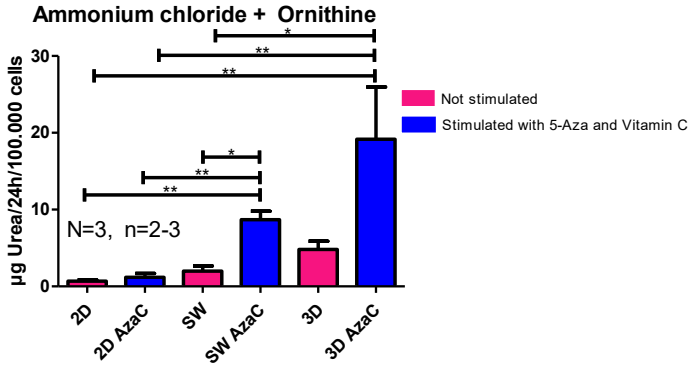

Figure 19: Urea production in a solution containing ammonium chloride as well as ornithine
Ammonia detoxification after 24 hours incubation in a basic solution by HepG2 cells in 2D, sandwich culture (SW) and on scaffolds (3D). Blue bars represent cells stimulated for 48 hours with 10 µM 5-Aza and 0.5 mM Vitamin C, while blue bars represent cells not stimulated. The ammonia detoxification was quantified by determining the urea production in 24 hours. The values were normalized to cell number determined by resazurin conversion assay. Bars represent mean ±SEM; N = 3, n = 3.

The lowest activity in this measurement was detected in the unstimulated 2D culture, while the highest activity was measured in the 3d culture stimulated with AzaC.

Comparing the unstimulated 2D culture with the unstimulated sandwich culture, we saw no statistically significant increase in activity, however, the AzaC sandwich culture was significantly higher than the unstimulated 2D culture (**). Similarly, there was no significant difference between the unstimulated 2D culture and the unstimulated 3D culture, despite the latter showing higher activity. The AzaC 3D culture, however, was significantly higher than the unstimulated 2D culture (**). Despite seeing higher activity in the unstimulated 3D culture compared to the unstimulated sandwich culture, this

difference was not statistically significant. We did, however, see a significant increase in activity in the AzaC 3D culture when comparing to the unstimulated sandwich culture. When comparing the AzaC 2D culture to the unstimulated 2D culture, no significant difference was found in the activity. However, the AzaC sandwich culture showed significantly more activity than the unstimulated sandwich culture (*). Although a higher activity showed in the AzaC 3D culture when compared to the unstimulated 3D culture, this effect was not statistically significant. This may be due to the high standard error of the mean in the AzaC 3D culture. However, Grubb's test did not reveal any outliers in the AzaC 3D data set.

To summarize, we saw an increase in urea production in the AzaC culture conditions when compared to their unstimulated counterparts in sandwich and 3D, although this was only statistically significant for the sandwich culture. In addition, we also found an increase in activity in both sandwich and 3D culture, when compared to unstimulated 2D culture, although this was only significant in the AzaC conditions for 3D and sandwich. When looking at U1, U2 and U3 combined, we saw an increase in urea production in both sandwich culture as well as 3D culture when compared to 2D culture. Similarly, when comparing the AzaC groups to their unstimulated counterparts, we saw an increase in the AzaC groups, which was for the most part not statistically significant.

3.2.2 CYP activity

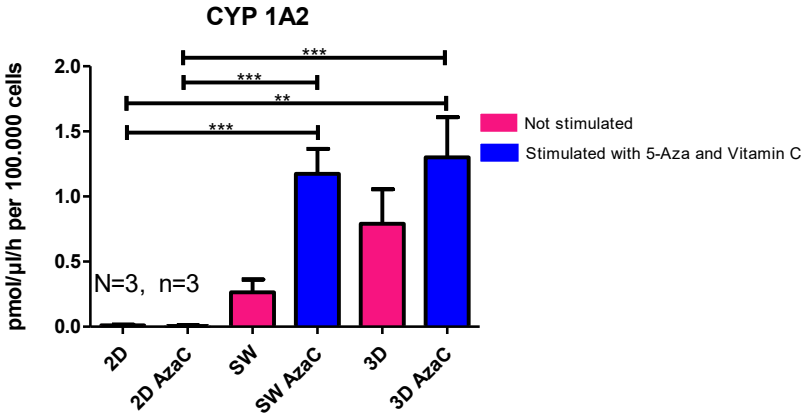

Figure 20: CYP1A2 activity in a basic solution by HepG2 cells in 2D, sandwich culture (SW) and on scaffolds (3D). Blue bars represent cells stimulated for 48 hours with 10 µM 5-Aza and 0.5 mM Vitamin C, while blue bars represent cells not stimulated. The activity was determined by measuring the relevant reaction products in the supernatant after 30 minutes. The values were normalized to cell number determined by resazurin conversion assay. Bars represent mean ± SEM; N = 3, n = 3.

The lowest measurements of CYP1A2 activity were in both the unstimulated and the AzaC 2D cultures. The highest activity was detected in the AzaC 3D culture, with the AzaC sandwich culture showing nearly as much activity. Significantly higher activity was measured in cells stimulated with AzaC in sandwich culture compared to both AzaC and unstimulated 2D culture. Analogously, the activity in the AzaC 3D culture was significantly higher in relation to AzaC and unstimulated 2D culture. No significant difference was detected between the unstimulated and the AzaC cultures of the same culture type, although there is a non-significant difference in both the 3D and the sandwich culture when comparing the AzaC with the unstimulated cultures.

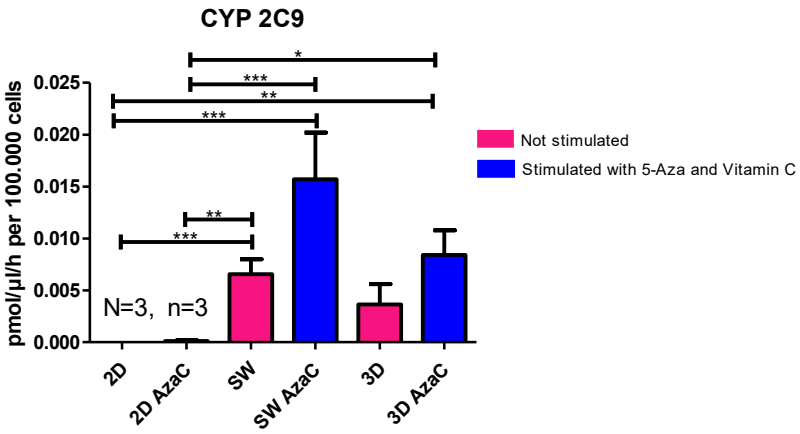

Figure 21: CYP2C9 activity in a basic solution by HepG2 cells in 2D, sandwich culture (SW) and on scaffolds (3D). Blue bars represent cells stimulated for 48 hours with 10 µM 5-Aza and 0.5 mM Vitamin C, while blue bars represent cells not stimulated. The activity was determined by measuring the relevant reaction products in the supernatant after 30 minutes. The values were normalized to cell number determined by resazurin conversion assay. Bars represent mean ± SEM; N = 3, n = 3.

In the measurement of the CYP2C9 activity, both 2D culture conditions display very low activity. The highest activity was in the AzaC sandwich culture.

When comparing the unstimulated 2D culture to sandwich culture, both the AzaC and the unstimulated sandwich culture show significantly higher activity (***). In addition, unstimulated sandwich culture shows significantly higher activity than AzaC 2D culture (**) and stimulated sandwich culture also measured significantly higher than AzaC 2D culture (***). While unstimulated 3D culture showed higher activity than unstimulated 2D culture, this effect was not statistically significant. However, AzaC 3D culture showed significantly higher activity than both unstimulated 2D culture (**) as well as AzaC 2D culture (*).

Unstimulated 2D culture and AzaC 2D culture both showed very low activity, and no significant difference was found. Comparing unstimulated sandwich culture to AzaC

sandwich culture, the AzaC group showed much higher activity, however, this was not statistically significant, due to a high standard error of the mean in the AzaC sandwich culture. Grubb's test did not reveal any outliers in either of the data sets. Similarly, in the comparison between AzaC 3D culture and unstimulated 3D culture, while the AzaC culture had higher activity, this was not significant.

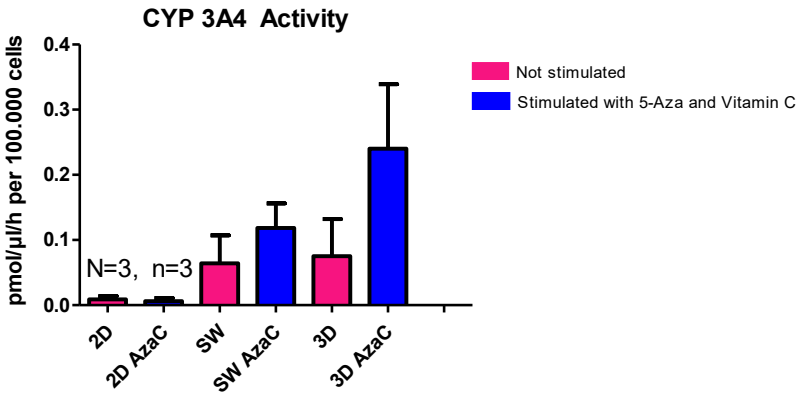

Figure 22: CYP3A4 activity in a basic solution by HepG2 cells in 2D, sandwich culture (SW) and on scaffolds (3D). Blue bars represent cells stimulated for 48 hours with 10 µM 5-Aza and 0.5 mM Vitamin C, while blue bars represent cells not stimulated. The activity was determined by measuring the relevant reaction products in the supernatant after 30 minutes. The values were normalized to cell number determined by resazurin conversion assay. Bars represent mean ± SEM; N = 3, n = 3.

For CYP3A4, both the unstimulated and the AzaC 2D conditions showed the lowest activity, while the AzaC 3D culture showed the highest activity measured. Comparing the unstimulated 2D culture with the unstimulated sandwich culture, the sandwich culture showed higher activity, albeit not statistically significant. Similarly, comparing unstimulated 2D culture to unstimulated 3D culture showed no statistically significant difference, despite the unstimulated 3D showing higher activity. Between unstimulated sandwich and unstimulated 3D culture, no significant difference was found. Between the AzaC 2D and the unstimulated 2D culture, no significant difference could be found either. While the AzaC sandwich culture showed higher activity, this was not statistically significant. Similarly, the activity of 3D AzaC appeared much higher than that of unstimulated 3D culture. When looking at the data generated in the cell culture experiments, it becomes apparent, that especially in 2D, very little activity was detected, with many of the wells showing no detectable activity.

In summary, sandwich culture showed higher activity than 2D culture for all three of the CYP enzymes, which was significant for CYP2C9. Additionally, the cells cultured in 3D showed higher activity of CYP enzymes, this similarly was statistically significant for

CYP2C9. While the cells stimulated with AzaC appear to have higher activity when compared to their unstimulated counterparts, this was not statistically significant.

3.2.3 UGT / GST

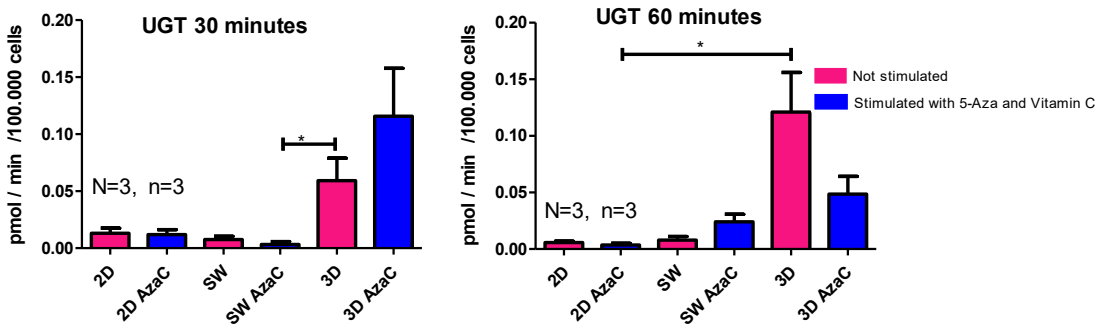

Figure 23: UGT activity after 30 and after 60 minutes by HepG2 cells in 2D, sandwich culture (SW) and on scaffolds (3D). Blue bars represent cells stimulated for 48 hours with 10 µM 5-Aza and 0.5 mM Vitamin C, while blue bars represent cells not stimulated. The activity was determined by measuring the concentration of 4-Methylumbelliferone in the supernatant after 30 minutes and after 60 minutes. The values were normalized to cell number determined by resazurin conversion assay. Bars represent mean ± SEM.

At both the 30-minute and at the 60-minute time point, AzaC and unstimulated 2D culture as well as the unstimulated sandwich culture show very little activity. The 3D culture conditions show more activity, albeit with large standard deviations. Accordingly, the only significant difference is between the unstimulated 3D culture and the AzaC sandwich (at the 30-minute time point) and the AzaC 2D culture (at 60 minutes).

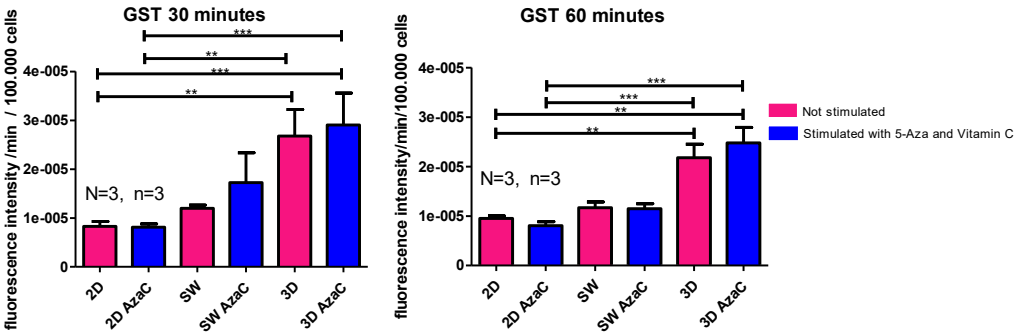

Figure 24: GST activity after 30 and after 60 minutes by HepG2 cells in 2D, sandwich culture (SW) and on scaffolds (3D). Blue bars represent cells stimulated for 48 hours with 10 µM 5-Aza and 0.5 mM Vitamin C, while blue bars represent cells not stimulated. The activity was determined by measuring fluorescence at excitation 355 nm and

emission 460 nm in the supernatant after 30 minutes and after 60 minutes. The values were normalized to cell number determined by resazurin conversion assay. Bars represent mean ± SEM; N = 3, n = 3.

The lowest activity for the GST measurement was detected in the AzaC 2D culture for both 30 minutes and 60 minutes. The highest activity was detected at both timepoints in the AzaC 3D culture. At both time points, there was a significant difference between the AzaC 3D culture and both the AzaC and the unstimulated 2D cultures. Equally, the unstimulated 3D culture showed a significantly higher activity of GST compared to both the AzaC and the unstimulated 2D culture. Neither sandwich culture showed a significant difference in GST activity when compared to the other culture conditions at either time point.

3.2.4 Efflux assays

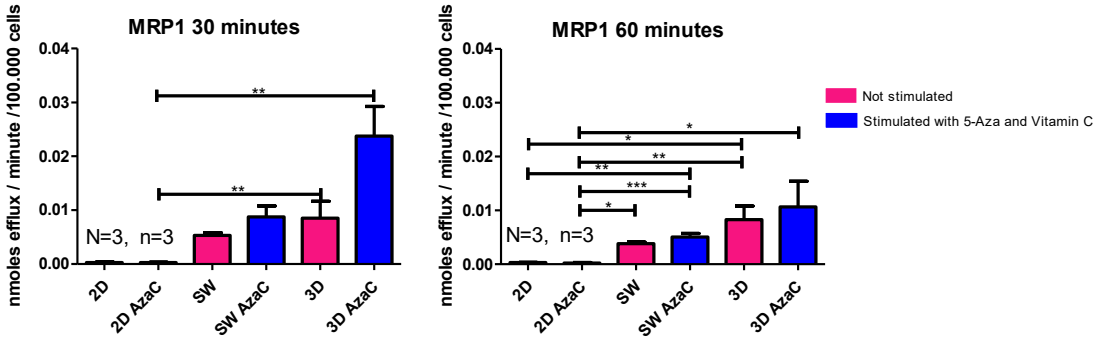

Figure 25: MRP1 activity after 30 and after 60 minutes by HepG2 cells in 2D, sandwich culture (SW) and on scaffolds (3D). Blue bars represent cells stimulated for 48 hours with 10 µM 5-Aza and 0.5 mM Vitamin C, while blue bars represent cells not stimulated. The activity was determined by measuring the concentration of 5-Carboxyfluorescein after 30 minutes and after 60 minutes. The values were normalized to cell number determined by resazurin conversion assay. Bars represent mean ± SEM; N = 3, n = 3.

At both timepoints, both the AzaC and the unstimulated 2D cultures showed the lowest activity of the MRP1-transporter. The highest efflux at both timepoints was measured in the AzaC 3D culture. At the 30-minute timepoint the unstimulated 3D culture showed a significantly higher activity than the AzaC 2D culture. Equally, the AzaC 3D culture showed a significantly higher activity when compared to the AzaC 2D condition.
At the 60-minute timepoint, the AzaC 3D culture showed a significantly higher activity than the AzaC 2D culture as well. Compared to both the AzaC and the unstimulated 2D cultures, the unstimulated 3D culture showed a significant increase in efflux activity at the 60-minute timepoint. Analogously, the AzaC sandwich showed a significantly higher activity compared to both of the 2D conditions. The unstimulated sandwich showed a

significant difference to the AzaC 2D culture. Overall, the activity per minute was markedly lower at the 60-minute timepoint compared to the 30-minute timepoint.
No significant increase in MRP1-transporter activity was detected between the AzaC and the unstimulated culture conditions of the same modality at either timepoint. However, the measurements of the AzaC culture conditions appear to be higher than their corresponding counterparts at both timepoints.

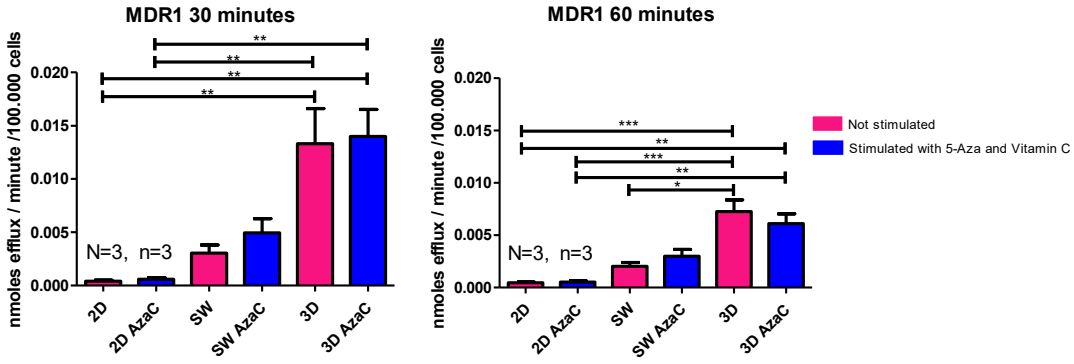

Figure 26: MDR1 activity after 30 and after 60 minutes by HepG2 cells in 2D, sandwich culture (SW) and on scaffolds (3D). Blue bars represent cells stimulated for 48 hours with 10 µM 5-Aza and 0.5 mM Vitamin C, while blue bars represent cells not stimulated. The activity was determined by measuring the concentration of p-glycoprotein after 30 minutes and after 60 minutes. The values were normalized to cell number determined by resazurin conversion assay. Bars represent mean ± SEM; N = 3, n = 3.

Both at the 30-minute as well as at the 60-minute timepoint the lowest activity was detected in both the AzaC as well as in the unstimulated 2D cultures. The AzaC and the unstimulated 3D cultures showed the highest activity at both timepoints, with the unstimulated 3D showing the highest activity at 30 minutes and the AzaC 3D the highest at 60 minutes.

The AzaC 3D showed a significantly higher activity than both the AzaC and the unstimulated 2D culture at both time points. The unstimulated 3D culture equally showed a significant increase in activity compared to both 2D cultures. There was also a significantly higher MDR1-activity when compared to the unstimulated sandwich culture.There was no significant difference in MDR1-activity when comparing the AzaC vs. the unstimulated conditions of corresponding culture modalities.The sandwich culture, albeit showing higher activity compared to the 2D culture, showed no significant increase to 2D. The efflux activity per minute was lower at the 60 minute timepoint compared to the 30 minute timepoint on average for all culture conditions.

3.3 PCR

3.3.1 Preparatory tests for PCR

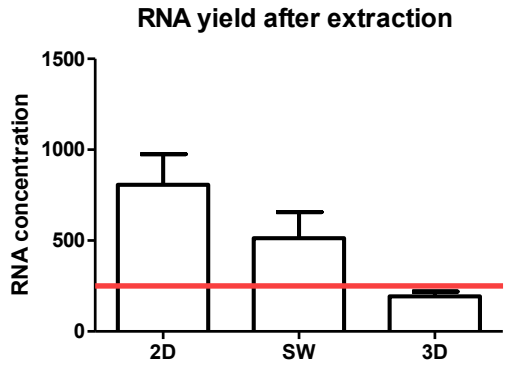

Figure 27: RNA yield from cells cultured on different mechanical substrates. The red line represents the minimum RNA yield required to create a standardized testing mix for semi-quantitative PCR

Figure 27 shows the RNA yield after 48 hours of stimulation, determined using the LVIS plate in the plate reader. The red line represents the minimum required concentration of 250 ng/µl. While samples from 2D and sandwich culture had sufficient concentrations of RNA, most samples from 3D culture had concentrations below those required to perform PCR.

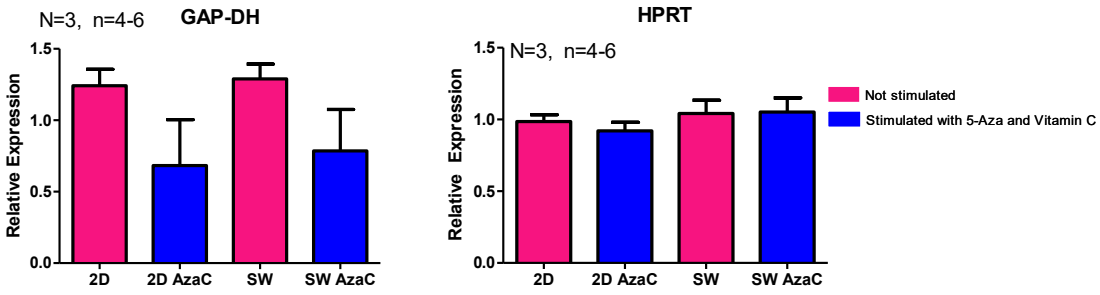

Figure 28: Gel electrophoresis of GAP-DH and HPRT from the same samples in 2D culture and sandwich (SW) culture. Blue bars represent cells stimulated for 48 hours with 10 µM 5-Aza and 0.5 mM Vitamin C, while blue bars represent cells not stimulated. Bars represent mean ± SEM; N = 3, n = 4-6.

The expression of *GAP-DH* varied markedly between the different culture conditions. Interestingly, the samples that had been stimulated with AzaC seemed to have a lower expression of *GAP-DH*, albeit not significantly due to low replicate number and large standard deviations.

For *HPRT* the difference between the expression of the samples was much smaller and *HPRT* was thus chosen for normalization of the gene expression data.

3.3.2 PCR Results

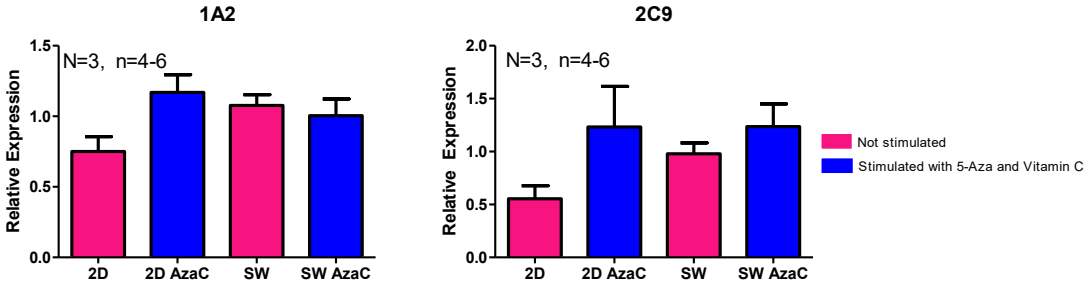

Figure 29: Expression levels of CYP 1A2 and CYP 2C9 for 2D and sandwich (SW) culture.
Blue bars represent cells stimulated for 48 hours with 10 µM 5-Aza and 0.5 mM Vitamin C, while blue bars represent cells not stimulated. The values were normalized to the expression of HPRT in the same sample. Bars represent mean ± SEM; N = 3, n = 4-6. No statistical significance was found

Figure 29 shows the results of PCR followed by gel electrophoresis for *CYP1A2* and *CYP2C9* in relative expression. Values have been normalized to *HPRT* expression.

For *CYP1A2,* there were no significant differences between the samples. The unstimulated 2D sample had the lowest expression for *CYP1A2*, while the AzaC 2D culture had the highest expression. AzaC 2D culture showed a 1.5-fold increase in expression of *CYP1A2* compared to unstimulated 2D culture. Unstimulated Sandwich culture showed a 1.4-fold increase in expression compared to unstimulated 2D culture. AzaC sandwich culture and unstimulated sandwich culture showed comparable expression of *CYP1A2*.

For *CYP2C9* expression, there were no significant differences between any of the culture conditions either. The unstimulated 2D sample had the lowest expression here as well, with the relative expression of the AzaC 2D and the AzaC sandwich being roughly equal. AzaC 2D culture showed a 2.2-fold higher expression of *CYP2C9* than unstimulated 2D culture. Similarly, unstimulated sandwich culture showed a 1.7-fold higher expression compared to unstimulated 2D culture. There was only a 1.2-fold increase in expression in AzaC sandwich culture compared to unstimulated sandwich culture.

For *CYP3D4,* PCR was performed to investigate expression levels, but no expression could be detected in any of the experimental samples. This is in line with the findings of Wilkening *et al.*, who detected no measurable expression of *CYP3A4* in HepG2 cells (Wilkening *et al.*, 2003).

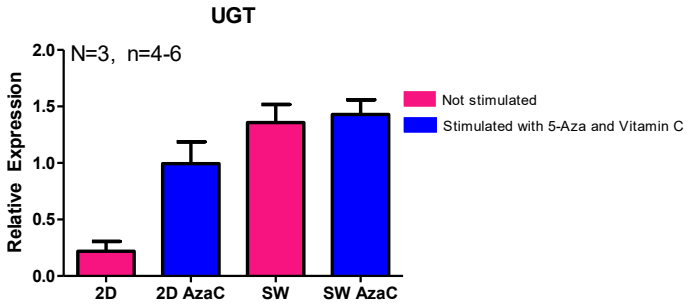

Figure 30: Expression levels of UGT for 2D and sandwich (SW) culture.
Blue bars represent cells stimulated for 48 hours with 10 µM 5-Aza and 0.5 mM Vitamin C, while blue bars represent cells not stimulated. The values were normalized to the expression of HPRT in the same sample. Bars represent mean ± SEM; N = 3, n = 4-6. No statistical significance was found

The unstimulated 2D culture showed the lowest expression of *UGT* of all the samples. The highest expression was seen in the AzaC sandwich culture. Both the AzaC 2D and the AzaC sandwich culture showed a higher expression of *UGT*, albeit not statistically significant.

Compared to unstimulated 2D culture, the AzaC 2D group showed a 4.5-fold higher expression of *UGT*. The unstimulated sandwich culture showed a 6.2-fold higher expression compared to unstimulated 2D culture. Between AzaC sandwich culture and unstimulated sandwich culture, the expression was comparable.

No expression of *GST* could be detected in any of the samples.

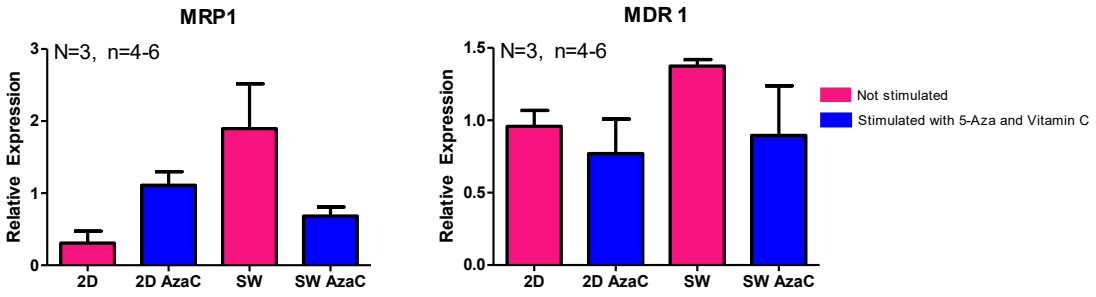

Figure 31: Expression levels of MRP1 and MDR1 for 2D and sandwich (SW) culture.
Blue bars represent cells stimulated for 48 hours with 10 µM 5-Aza and 0.5 mM Vitamin C, while blue bars represent cells not stimulated. The values were normalized to the expression of HPRT in the same sample. Bars represent mean ± SEM; N = 3, n = 4-6 No statistically significant difference was found.

For *MRP1*, the sample with the lowest expression was the unstimulated 2D culture with the unstimulated sandwich culture showing the highest expression. No statistically significant difference between the sample could be found.

The AzaC 2D culture showed a 3.6-fold higher expression of *MRP1* compared to unstimulated 2D culture. Unstimulated sandwich culture showed a 5.1-fold higher expression compared to unstimulated 2D culture. Interestingly, when comparing the

AzaC sandwich group with the unstimulated sandwich group, the unstimulated sandwich group showed a 2.3-fold higher expression than the AzaC group.

The lowest expression of *MDR1* in the investigated samples was the AzaC 2D culture. The highest expression of *MDR1* was shown by unstimulated sandwich culture. The difference between the expression of the samples was not statistically significant, however, the AzaC samples showed a lower expression than their unstimulated counterparts. In comparison to the unstimulated 2D group, the unstimulated sandwich group showed a 1.4-fold higher expression of *MDR1*.

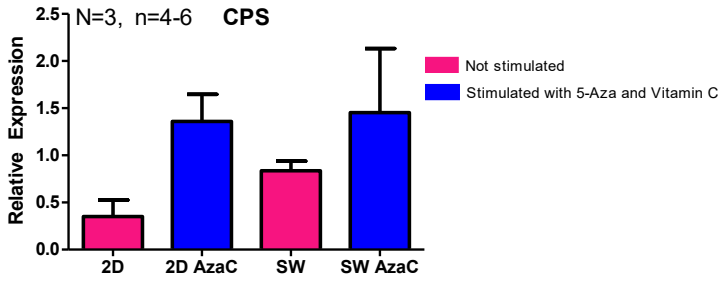

Figure 32: Expression levels of CPS for 2D and sandwich (SW) culture.
Blue bars represent cells stimulated for 48 hours with 10 µM 5-Aza and 0.5 mM Vitamin C, while blue bars represent cells not stimulated. The values were normalized to the expression of HPRT in the same sample. Bars represent mean ± SEM; N = 3, n = 4-6. No statistically significant difference was found.

For *CPS,* the lowest expression was detected in the unstimulated 2D samples. The AzaC culture conditions showed a higher expression than their corresponding counterparts, albeit not statistically significant. The unstimulated sandwich culture showed a higher expression than the unstimulated 2D culture, although not statistically significant. Comparing the AzaC 2D culture to the unstimulated 2D culture, a 3,8-fold higher expression of *CPS* in the AzaC group was found. The unstimulated sandwich culture showed a 2.3-fold higher expression than the unstimulated 2D culture. When comparing the AzaC sandwich culture to the unstimulated sandwich culture, the AzaC culture condition showed a 1.7-fold higher expression.

In summary, we saw an 1.5-4.5-fold increase in AzaC 2D culture compared to its unstimulated counterpart in the expression of the genes investigated apart from *MDR1*. Similarly, we saw a higher expression of all genes investigated in unstimulated sandwich culture when comparing to unstimulated 2D culture.

4 Discussion

In this study, we aimed to investigate two distinct methods of improving hepatocyte-like function in HepG2 cells.

This cell-line shows stable hepatocyte-like enzyme activity, albeit on a much-reduced level (Wilkening *et al.*, 2003). The difference to pHH in activity and gene expression is due to several factors, among them epithelial-mesenchymal transition, which occurs due to a marked difference in gene expression and epigenetics in HepG2 (Ruoß *et al.*, 2019). As it has been shown in the past, 5-Azacytidine and vitamin C can partially reverse the effects of EMT (Sajadian *et al.*, 2016). We aimed to show that this changed epigenetic behavior also leads to a higher activity of several key hepatocyte-specific enzymes.

Beyond that, as a second experimental approach, our aim was to investigate the effect of scaffold 3D-culture on these same enzymes. Scaffolds are a promising avenue in tissue engineering and are expected to improve several shortcomings of classical 2D culture in pHH, such as the rapid decline in morphology and function. To set a baseline for our 3D-experiments, we also employed collagen sandwich culture, a well-established, very simple, approach that has been shown to prolong pHH-survival *in vitro* and has been utilized as a comparison when establishing more complex 3D methods (Dunn *et al.*, 1989).

For all our 3D experiments, we used HepG2 cells, as their wide availability and general resilience in culture makes them an ideal prospect for establishing this culture method (Wilkening *et al.*, 2003). As described in the introduction, there are several different approaches to 3D cultures, ranging from 3D-printed scaffolds over hydrogels and cryogels to decellularized tissue samples (Godoy *et al.*, 2013).

Our approach of a protein- and polymer- based cryogel has several key advantages for the purpose of scaffold creation; Firstly, the materials are all readily available and the scaffold creation is comparatively simple, so that a sufficient number of scaffolds can be created for experimentation. Secondly, as all materials involved have been used in cell-culture-based experiments for many years, they have a proven high degree of biocompatibility (Carvalho *et al.*, 2014; Godoy *et al.*, 2013; Park *et al.*, 2004; Ruoß *et al.*, 2020).

Additionally, with the option of varying the composition of scaffolds or adapting the polymerization process, it can easily be changed or adapted to future experimental

requirements, such as a variation of stiffness or incorporation of additional substrates into the scaffold matrix (Häussling *et al.*, 2019; Ruoß *et al.*, 2020).

None of the scaffolds we investigated showed any macroscopic degradation when exposed to the substances required to use in cell culture. However, the scaffold from composition 2, which was created without gelatin, was much less mechanically stable and prone to breaking apart when transferred.

Furthermore, the creation of pores as a vital part of the scaffolds interior surface was shown.

The diameter of pores in and on the scaffold is an important factor in allowing cells to penetrate further into the scaffold and to provide them with nutrients and medium (Kumari *et al.*, 2016). We found that all four investigated scaffold compositions showed sufficient pore diameter to allow for nutrients and cells to pass through, with the average diameter being between 95,7 – 176,3 µm. As a comparison, the pore size in decellularized liver is around 22.02 ± 0.65 µm, although it has been shown that this also depends on other factors such as wetness of the scaffold (Mattei *et al.*, 2018).

Interestingly, in all four investigated compositions, we found long, mostly vertical pores toward the outer edges of the scaffold. Oelschlaeger *et al.* found a connection between the formation of more interconnected pores with thinner walls to the polymerization time (Oelschlaeger *et al.*, 2016). As the outer parts of the scaffold solution cool down the fastest, thus having the shortest polymerization time, the vertical pores might be caused by a shorter polymerization period. In the compositions with a higher content of pHEMA or protein as part of the polymerization solution, which were compositions 3 and 4, we found much smaller pores as well as thicker pore walls. In composition 4, the pores did not form an interconnected network.

Composition 1 was chosen for further testing, as it was mechanically stable, had a good porosity and a high reproducibility.

We saw that a step of pre-treating the scaffolds with medium containing FCS and P/S was a vital step in scaffold preparation as it allowed the adherence of a much higher number of viable cells onto the scaffold surface. This matches similar finds regarding the pre-treatment of scaffolds by Kumari *et al.* (Kumari *et al.*, 2016).

Our cells, when seeded with the surface seeding technique did not penetrate further than a few µm into the scaffolds. As the cells are supposed to not only adhere to the surface of the scaffold, but to the pore walls deep inside the scaffold as well, we investigated several methods of seeding. In surface seeding, a solution containing cells is pipetted on top of

the scaffold, while in orbital seeding, the scaffold is submerged in a cell solution, which is then continuously gently agitated. Orbital seeding can potentially distribute the cells more evenly across a surface. Major drawbacks of orbital seeding include the high cell number required as well as the practical imposition of not being able to agitate the cell solution within the incubator (Melke *et al.*, 2020).
Fluorescence microscopy of scaffolds seeded with the orbital seeding method as well as with the classic surface seeding method showed that in both cases cells adhered only to the surface of the scaffold and did not migrate deeper into the scaffold. Additionally, the number of cells on the scaffold after orbital seeding appeared to be much less than after surface seeding. As a result, surface seeding was chosen for the experiments, although further refinement of an orbital seeding approach might yield better results.
In summary, we were able to establish a scaffold creation process from biocompatible materials, that showed reliable pore formation as well as good mechanical stability and could be used with our protocols for further cell-culture based testing.

With the scaffold, pre-treatment and seeding method established and the presence of cells on the scaffold verified, we moved on to metabolic experiments.
A key factor in these experiments is cell number quantification. A number of experimental approaches have been described in literature before this study and since, such as protein normalization, DNA quantification and assays such as MTT (Jones *et al.*, 2001; van Tonder *et al.*, 2015). The resazurin conversion assay utilized in this study has been used for cell quantification for a long time, although it has its limitations, as will be discussed further below (Uzarski *et al.*, 2017).

We were able to show an improvement of hepatocyte-like functionality in HepG2 cells in 3D culture, particularly in the activity of CYP1A2, CYP2C9, GST, MDR1 and MRP1, as well as for urea production. For the other metabolic tests, we saw an increase in activity in 3D as well, however not statistically significant. The next step in corroborating the results would have been mRNA extraction with the goal of matching PCR results with our metabolic data. However, as mRNA extraction from cryogels proved difficult, the resulting mRNA did not show the purity and integrity required for rtPCR (Sambrook *et al.*, 1989)
There are several studies of the effects of 3D culture on the metabolic activity in HepG2, especially of urea and albumin secretion, as these can readily be measured in supernatant.

Several of these have shown a positive effect of 3D culture on urea and albumin over up to 21 days (Luckert *et al.*, 2017; Meng *et al.*, 2020; Teng *et al.*, 2018). Luckert *et al.* also investigated the effects of an alginate-based scaffold on several CYP enzymes, finding a statistically significant increase in the activity of CYP1A2 and CYP2C9 (Luckert *et al.*, 2017), corroborating our results.

Another one of the aims of this study was to investigate the effect of sandwich culture on the metabolic activity of HepG2 cells.

Ramaiahgari *et al.* were able to show an increase in liver-specific gene expression, among them the genes investigated in this study, over a period of 28 days after cell seeding into Matrigel (Ramaiahgari *et al.*, 2014). However, a study performed by Luckert *et al.* investigating several 3D-culturing techniques found no increase in liver-specific activity on d21 in HepG2 sandwich culture. They did, however, find a more liver-like morphology with the formation of bile canaliculi (Luckert *et al.*, 2017).

In our study, we saw a significant increase in the activity of CYP2C9 and MRP1, which also corresponded with an increase in expression of each gene. We also saw a non-significant increase in activity for the other enzymes except GST, which was accompanied by an increase in gene expression. These findings correspond with Ramaiahgari *et al.,* however, with such limited data on the effects of sandwich, additional testing is required. While we saw an increase in gene-expression toward a more hepatocyte-like pattern, the mechanism of this change has not been investigated to date. As there are several mechanisms contributing to the expression pattern of HepG2, such as histone methylation and acetylation (Ruoß *et al.*, 2019), further investigation may provide insight, which of these are affected by sandwich culture and how they may further be improved. Additionally, more extensive studies as to the morphology of HepG2 cells in sandwich culture may contribute to understanding the mechanisms involved.

When comparing 3D data to sandwich data, we only saw a statistically significant increase in activity for urea production (U2), the other investigated enzymes, although showing an increase, were not statistically significant. There are few studies that investigate both sandwich and scaffold 3D culture. Luckert *et al.* found no significant difference between sandwich and scaffold culture for the CYP enzymes investigated (Luckert *et al.*, 2017).

The second aim of our study was to investigate the effect of stimulation with AzaC on the metabolic function of HepG2. Treatment with these two substances, which induce

epigenetic modification and a partial reversion of EMT, have been shown to improve hepatocyte-like-functionality in HepG2 (Ruoß *et al.*, 2019).

In the metabolic assays of our study, we did not find a significant increase in activity for our stimulated cell culture condition. In fact, when comparing any of the three culture conditions (2D, sandwich and 3D scaffold culture) with their respective stimulated counterparts, we could not detect a statistically significant increase in any of our experiments, despite stimulated conditions showing almost ubiquitously higher activity in 3D and sandwich culture. However, for several of the investigated genes (*CPS, CYP1A2, CYP2C9 MRP1* and *UGT*) we were able to see an increase in expression in the AzaC 2D condition, when compared to unstimulated 2D. For *MDR1*, the expression was decreased through stimulation.

These finding are in line with results published by Ruoß *et al.*, who also found an increase in the expression of *CYP1A2* and *CYP2C9* (Ruoß *et al.*, 2019). For the other genes, no published data exists .

As all these genes are expressed at a much lower level in HepG2, the increase in expression shows a positive effect on the epigenetic changes in this cell line, which moves them closer to the function of pHH. For *MDR1*, which is expressed higher in HepG2 than in pHH, the stimulation showed a positive effect by decreasing the expression in the stimulated samples. However, all of these changes remain on a low level when compared to the gap between HepG2 and pHH gene expression (Donato *et al.,* 2008).

To summarize, while we did see an increase in the expression of the investigated genes, the stimulation with 5-Aza and Vitamin C did not significantly increase the activity of the liver-specific enzymes investigated in this study in 2D culture. Research published by Sajadian *et al.* and Ruoß *et al.* indicate that the effect of 5-azacytidine, which in turn is enhanced by the addition of vitamin C, is TET-mediated and is accompanied by downregulation of EMT-associated genes such as *snail*, as well as upregulation of epithelial marker genes like *E-cadherin* an *HNFα* (Ruoß *et al.*, 2019; Sajadian *et al.*, 2015).

Of further interest to our study are the combined effects of either 3D scaffold culture or sandwich culture and stimulation with AzaC. In all the metabolic experiments, activity in AzaC 3D culture was higher than in unstimulated 3D culture, however, in none of the cases could a statistical significance be proven.

Similarly, we did not find a significant difference between AzaC sandwich culture and unstimulated sandwich culture in any of the metabolic tests, despite the AzaC group showing higher activity in many of them, particularly the CYP activity. For gene expression, *CYP2C9* as well as *CPS* were expressed at a higher level than in the unstimulated sandwich group.

When comparing AzaC 3D culture to the unstimulated 3D culture, we did not see a statistically significant difference either, despite AzaC 3D generally showing higher activity. Several studies have investigated the effect of either stimulation with AzaC (Ruoß *et al.*, 2019; ajadian *et al.*, 2016) or 3D-cultivation methods (Luckert *et al.*, 2017; Ramaiahgari *et al.*, 2014) on HepG2 cells, however, no study before has investigated the combined effect.

In summary, we were able to see an increase in metabolic function from both sandwich and 3D scaffold culture, with scaffold culture increasing function more than sandwich. While we were not able to detect a significant increase of activity in stimulated conditions, we did find an increased expression of several genes, that are generally expressed higher in pHH and a downregulation of *MDR1*. This indicates a generally positive effect of both investigated 3D culturing techniques on the hepatocyte-like function of HepG2 cells, a finding that is in line with past publications (Luckert *et al.*, 2017; Meng *et al.*, 2020; Teng *et al.*, 2018).

4.1 Limitations of methods

There are several aspects of this study that need to be considered when interpreting the results. As already discussed above, cell normalization was achieved using a resazurin conversion assay. While this method can give valuable information on cell viability and has seen long use as a means of determining cell number (Uzarski *et al.*, 2017), its use a method for the latter in 2D culture has been replaced by newer methods, such as protein quantification via SRB staining and DNA quantification (Ruoß *et al.*, 2019; Stewart *et al.*, 2000; Zimmermann *et al.*, 2016). This is due to the fact that the resazurin assay relies on an enzymatic conversion, which can be influenced by a number of factors, such as cell stress, and critically to our approach, surface stiffness (Ruoß *et al.*, 2019; Uzarski *et al.*, 2017).

Hence, while the conversion assay gives a good indication of the number of viable cells in culture, other methods should be evaluated for future use. Such approaches include

DNA quantification, ATP measurement and PCR-based methods (Ruoß *et al.*, 2019). Other methods, such as flow cytometry or the use of a counting chamber would require extensive optimization to ensure that the entirety of the cells on the scaffold is determined by the measurement, while protein-based methods such as Lowry assay or SRB staining are impractical due to the proteins used in scaffold creation.
Secondly, our focus in this study was to establish a scaffold with sufficient pore formation and to investigate its effects on metabolic function. Therefore, the stage of characterization and optimization prior to starting cell-culture tests, was limited. Even for a narrowly defined purpose, the scaffold should be thoroughly characterized, and its production optimized before moving onto pHH culture. We will discuss possible avenues of characterization and optimization further below.

In addition, some limitations in interpreting the data from this study became apparent. To further confirm the data collected in the metabolic tests, PCR and subsequent electrophoresis of key hepatocyte-specific genes would be required for all three culture modalities. For the scaffolds, however, mRNA extraction in a sufficient purity and integrity could not be achieved. For mRNA extraction, we crushed the shock-frozen scaffolds and then extracted the RNA using TriFast mix. However, as described above, both the yield and the purity of the mRNA recovered from the scaffolds proved insufficient for PCR. Hence, to improve the reliability of 3D-experimentation, a method for mRNA-extraction from scaffolds should be established.
Additionally, while our method of measuring gene expression, reverse transcriptase PCR (RT-PCR) followed by gel electrophoresis, is well-established and both convenient in handling and readily available, it is not the gold standard. This method is excellent as a means for qualitative investigations but remains “semi-quantitative” in nature. There are a number of factors that hamper its ability to detect differences in expression, especially for genes with low expression (Marone *et al.*, 2001, Chen, 1999). Each cycle doubles the amount of DNA in the sample, which can lead to imprecise quantification (Wilkening *et al.*, 2003). During PCR, an exponential phase is described, followed by a plateau phase at a higher number of cycles, in which quantification becomes unreliable.
Small variations of reagents or sample in the PCR mix can be amplified and overshadow small differences in the gene expression of the samples (Huggett *et al.*, 2015). To mitigate the effect of batch-to-batch variations in the amount of DNA in the original sample,

results of RT-PCR are normalized against a house-keeper gene, such as *GAP-DH* or *HPRT* (Eisenberg *et al.,* 2013*).*

These shortcomings make PCR a less-reliable method of gene expression quantification. Quantitative PCR (qPCR), on the other hand, is a method of fluorescence-based real time method of quantification with a much higher sensitivity (Lee *et al.*, 2006) and might be a better choice.

4.2 Outlook

Beyond applications in medical tissue engineering, 3D-culture methods of liver-specific cells also show promise for *in vitro*-experimentation, where they can help prolong hepatocyte function and may delay de-differentiation in culture. With such a goal in mind, the first steps into 3D-culture should focus on establishing a scaffold that can reliably be used for 3D-culture with cells such as HepG2 and then optimizing and characterizing it. Once the scaffold has been thoroughly established, experimentation can move on to pHH. Basic scaffold characterization involves evaluation of the scaffolds for mechanical stability, the formation of a pore network as well as the effects of different matrix components. Larger pores than found *in vivo* or in decellularized liver samples are necessitated by the transfer of both the cells and nutrients to the inside of the scaffold (Kumari *et al.*, 2016).

Pore formation and properties have been shown to be directly linked to polymerization conditions, such as temperature during polymerization as well as polymerization duration (Oelschlaeger *et al.*, 2016). Transfer of medium and cells requires an interlinked pore network, thus further research to show the presence of such interlinked pores may provide valuable data. This can be done using confocal 3D-microscopy, or with micro-CT-scanning (Mizutani *et al.*, 2012; Naeem *et al.*, 2019). Once the presence of a pore network has been shown, further testing should be done to find the optimal pore size for both cell and nutrient transfer. The size and shape of pores within the scaffold is influenced by several key factors, such as protein content, cooling temperature, cooling direction and the cross-linking agents used. Alternative experimental approaches to cooling the mixture during polymerization include cooling all components down to 4°C before adding the crosslinking agents TEMED and APS or achieving a more stable surrounding temperature by using an ethanol bath (Kumari *et al.*, 2016; Teng *et al.*, 2018). This step of scaffold characterization also includes study of porosity as well as diffusion properties (Fan *et al.*,

2015; Shimizu *et al.*, 2006). Both are major factors in how the cells interact with the scaffold as well as mass transfer into the scaffold.

Further possible avenues of research to investigate cell behavior and distribution are discussed below but are also majorly influenced by pore size and the formation of a connected network. A well-described factor for pHH-behavior *in vitro* is the stiffness of the surface they are seeded on (Xia *et al.*, 2020). The stiffness of physiological liver tissue is around 1.5–4.5 kPa with terminal liver fibrosis reaching as high up as 48 kPa (Xia *et al.*, 2020). With cell-culture plates having a stiffness several orders of magnitude higher than that of even cirrhotic liver, a major improvement of pHH-culture was pre-coating of cell-culture wells with collagen to decrease the stiffness and provide the cells with ECM-material for adhesion (Dunn *et al.*, 1989).

To measure the stiffness of scaffolds, several methods have been employed. Firstly, compression testing and comparison with physiological sampling can be done, although for liver cell culture this approach suffers from a high degree of error in the measurement, as the methods generally are not optimized for tissue with such high elasticity. Another approach might be transient elastographic methods, most commonly employed in diagnostics such as Fibroscan™ or, in some cases, magnetic resonance elastography (Everwien *et al.*, 2020; Patel *et al.*, 2014). This has the advantage of well-established measurements of both healthy, as well as fibrotic/cirrhotic tissue *in vivo* to act as a comparison. The method is, however, optimized for much larger quantities of tissue than those employed in scaffolds and would have to be further adapted. A very sensitive, albeit laborious, method is atomic force microscopy with a spherical probe (Xia *et al.*, 2020).

With an established protocol for scaffold creation, the next step is optimization of culture conditions. In our study, we investigated two of the most common seeding techniques, surface seeding and orbital seeding. Surface seeding, where cells are distributed over the scaffold via pipette, is the simplest form of seeding and results in large quantities of cells on one side of the scaffold, with few cells penetrating deeper into the scaffold or adherent to other surfaces.

The other modality we investigated, orbital/rotational seeding, has been shown to greatly improve cell penetration deeper into the scaffold (Mirzaeian *et al.*, 2020). In our findings, we could not replicate this for our scaffold with HepG2 cells. Major drawbacks of this method involve a higher number of cells required for seeding as well as a lower adherence-rate, as the agitation of the cell solution cannot easily be performed under

incubator conditions. Beyond the dynamic seeding method via orbital shaker that we employed, methods such as perfusion-based seeding, suction and magnetic distribution have been described (Melke *et al.*, 2020).

While the amount and localization of seeded cells can be very accurately controlled using injection seeding methods, the seeded cells usually cluster at the injection site and don't distribute further into the scaffold (Liu *et al.*, 2020).

As hepatocyte morphology is closely linked to function, a closer study of morphology of cells inside the scaffold brings insight into the behavior of cells seeded in 3D. *In vivo,* hepatocytes have a distinct zonal polarity, which is induced by the arrangement of cell-to-cell and cell-to-ECM contacts (Aumüller, 2010, p. 660-664). 3D cultures aim to mimic these conditions more closely than 2D or sandwich culture. Morphological studies can be done using fluorescence microscopy, although this approach suffers from strong fluorescence of the scaffold in the most commonly wavelengths. This makes the dyes used for marking specific intracellular proteins such as microtubule equally susceptible to being lost in the background fluorescence. Additionally, the possibilities of scanning electron microscopy (SEM) for displaying both cell structure as well as cell-matrix interactions are increasingly being investigated (Iandolo *et al.*, 2019).

Once imaging techniques have been thoroughly established, studies into distribution and proliferation, either of immortalized cells like HepG2 or of pHH, can be done. As a key part of pHH dedifferentiation is their morphological deterioration, such studies could provide important evidence toward the efficacy of 3D culture. Functional assays are an important part in assessing the effects of 3D culture. To establish protocols for these assays, cell quantification needs to be thoroughly optimized. Resorufin conversion provides a good basis for cell quantification, but it can be inaccurate due to several factors, such as cell stress or surface stiffness (Ruoß *et al.*, 2019; Uzarski *et al.*, 2017). Other methods, such as protein quantification are impractical for our protein-based scaffold. A promising approach is cell quantification by measuring DNA content after lysing of the cells (Ruoß *et al.*, 2019). With accurate cell numbers, activity assays can be performed. Urea and albumin synthesis are the most widely spread tests for testing liver-like function in 3D, as the samples can be taken from the supernatant (Meng *et al.*, 2020). Other functional assays, such as phase I and phase II activity assays can also be performed, although they are highly dependent on sufficient mass transfer of test substances (Fan *et al.*, 2015; Shimizu *et al.*, 2006).

As one of the key challenges of *in vitro* research is the dedifferentiation and loss of

function of hepatocytes, long-term studies of 3D-cultured hepatocytes are a way to investigate, whether 3D culture can improve hepatocyte function enough to justify its much higher complexity as well as cost of culturing cells.

5 Summary

Primary human hepatocytes are the gold standard for *in vitro* toxicity testing, however, in classical 2D culture, they dedifferentiate rapidly, necessitating research into new culture modalities as well as alternative cell lines.

In this study we investigated the effects of sandwich and cryogel 3D culture as well as stimulation with 5-azacytidine in combination with vitamin C on the metabolic activity of HepG2 cells, an immortalized hepatoma cell that has been shown to maintain residual hepatocyte-like function. We created a scaffold from pHEMA, bis-acrylamide, collagen, cold fish gelatin, cross-linked by APS and TEMED. We were able to show regular pore formation and established a protocol for cell seeding and cell culture.

We were able to see an increase in the activity of several key enzymes in 3D and sandwich culture and we could also demonstrate an increase in gene expression as a result of epigenetic modification with AzaC as well as sandwich cultivation. Despite seeing higher activity, we could not detect a significant difference when comparing AzaC 3D culture with unstimulated 3D culture.

3D culturing of primary human hepatocytes offers promising avenues of research, but first, scaffolds need to be thoroughly optimized to mimic *in vivo* conditions as closely as possible.

6 Zusammenfassung

Primäre humane Hepatozyten sind der Goldstandard für *In-vitro*-Toxizitätstests, jedoch de-differenzieren sie in der klassischen 2D-Kultur sehr schnell, was die Erforschung neuer Kulturmodalitäten sowie alternativer Zelllinien erforderlich macht.
In dieser Studie untersuchten wir die Auswirkungen einer Sandwich- und einer Kryogel-3D-Kultur (Scaffolds) sowie der Stimulation mit 5-Azazytidin in Kombination mit Vitamin C auf die metabolische Aktivität von HepG2-Zellen, einer immortalisierten Hepatomzelllinie, die eine Restaktivität von hepatozytentypischer Funktion aufrechterhält.
Wir erstellten ein Protokoll für ein Cryogel aus pHEMA, Bis-Acrylamid, Collagen, sowie Gelatine, vernetzt von APS und TEMED. Wir konnten eine gleichmäßige Porenbildung nachweisen und ein Protokoll für die Zellaussaat und Zellkultur erstellen.
In unseren Experimenten sahen wir eine Erhöhung der Aktivität mehrerer Schlüsselenzyme in 3D- und Sandwich-Kulturen sowie eine Erhöhung der Genexpression durch epigenetische Modifikation mit AzaC. Trotz der höheren Aktivität konnten wir eine statistische Signifikanz des Unterschiedes nicht beweisen.
Die 3D-Kultivierung primärer humaner Hepatozyten bietet vielversprechende Forschungsmöglichkeiten, aber zunächst müssen die Scaffolds umfangreich optimiert werden, um die *In-vivo*-Bedingungen so genau wie möglich nachzuahmen.

7 List of abbreviations

2D	2-dimensional
3D	3-dimensional
4-MU	4-Methylumbelliferone
5-Aza	5-Azacytidine
5-CDFA	5(6)-Carboxy-2',7'-dichlorofluorescein diacetate
5-CF	5-Carboxyfluorescein
5hmC	5-hydroxymethyl cytosine
5mC	Methylation of cytosine in position 5
ABC	Antigen-Binding-Cassette
ABCB1	Antigen-Binding-Cassette B1
ABCC1	Antigen-Binding-Cassette C1
ALF	Acute liver failure
APAP	Acetaminophen
APS	Ammonium persulfate
AzaC	5-Aza and Vitamin C
BAA	bis-Acrylamide
Calcein AM	Calcein acetoxymethyl ester
°C	Degree Celsius
CPS	Carbamoyl phosphate synthetase
cDNA	Complementary DNA
CO_2	Carbon dioxide
CYP	Cytochrome p450
DAPI	4,6-Diamidin-2-phenylindol
ddH_20	Double distilled Water
DEPC H_2O	Diethyl carbonate water
DILI	Drug induced liver injury
DMEM	Dulbecco's Modified Eagle's Medium
DNA	Deoxyribonucleic Acid
DPBS	Dulbecco's Phosphate Buffered Saline
EM	Electron microscopy
EMA	European Medicines Agency
FCS	Fetal Calf Serum

FDA	Federal Drug Administration
g	Acceleration of gravity
g	Gram
GA	Glutaraldehyde
GAP-DH	Glycerinaldehyd-3-phosphat-Dehydrogenase
GFP	Green fluorescent channel
GST	Glutathione-S-transferase
h	Hour
H_2SO_4	Sulfuric acid
HPRT	Hypoxanthin guanine phosphoribosyl transferase
IVIVE	*In vitro* to *in vivo* extrapolation
kg	Kilogram
l	Litre
MCB	Monochlorobimane
MDR1	Multidrug Resistance Protein 1
$MgCl_2$	Magnesium chloride
mm	Millimeter
mM	Millimolar
mRNA	Messenger RNA
MRP1	Multidrug resistance related Protein 1
µl	Microliter
µM	Micromolar
NaOH	Sodium Hydroxide
NED	N-(1-naphthyl) ethylenediamine dihydrochloride
NH_4Cl	Ammonium chloride
NPC	Nonparenchymal cells
PCR	Polymerase chain reaction
pHEMA	Poly-(2-hydroxyethyl-methacrylat)
pHH	Primary human hepatocytes
P/S	Penicillin/Streptomycin
qPCR	Quantitative PCR
RT-PCR	Reverse transcriptase PCR
RNA	Ribonucleic acid
SEM	Standard error of the mean

SRB	Sulforhodamine B
T/E	Trypsin/EDTA
TEMED	Tetramethylethylendiamine
TET	Ten-eleven-transferases
TNFα	Tumor necrosis factor α
UDP	Uridine diphosphate
UGT	Uridine diphosphate glucoronosyl-transferase
V	Volt

8 Appendices

8.1 Primers used:

The following primers were used for PCR:

Glycerinaldehyde-3-phosphate-Dehydrogenase (NM_002046.4):

T_A: 56 °C / Cycles: 35 / Product size: 420 bp

F: GTCAGTGGTGGACCTGACCT

R: AGGGGTCTACATGGCAACTG

Cytochrome P450 1A2 (NM_000761.3):

T_A: 60 °C / Cycles: 30 / Product size 180 bp

F: TCGACCCTTACAATCAGGTGG

R: GCAGGTAGCGAAGGATGGG

Cytochrome P450 2C9 (NM_000771.3):

T_A: 59 °C / Cycles: 40 / Product size: 308 bp

F: CTGGATGAAGGTGGCAATTT

R: AGATGGATAATGCCCCAGAG

Cytochrome P450 3A4 (NM_017460.5):

T_A: 64°C / Cycles: 30 / Product size: 314 bp

F: ATTCAGCAACAAGAACAAGGACA

R: TGGTGTTCTCAGGCACAGAT

Carbamoyl-Phosphate Synthase 1 (NM_001122633.2):

T_A: 58 °C / Cycles: 35 / Product size: 272 bp

F: AGCCGAGGCCCATGCCACAA

R: TGGGTACCCTCCCAGGCCAGTA

Multidrug resistance 1 (NM_000927.4):

T_A: 61 °C / Cycles: 30 / Product size: 252 bp

F: ATCCGGGCCGGGAGCAGTCA

R: ATTCCGACCTCGCGCTCCTTG

Multidrug resistance protein 1 (NM_004996.3):

T_A: 58 °C / Cycles: 30 / Product size: 247 bp

F: TTGGATGAGGCCACGGCAGC

R: CTGGGGCTCACACCAAGCCG

UPD-Glucuronosyltransferase 1A6 (NM_001072):

T_A: 60 °C / Cycles: 35 / Product size: 210 bp

F: TGGTGCCTGAAGTTAATTTGCT

R: GCTCTGGCAGTTGATGAAGTA

Glutathion S-transferase alpha 1 (NM_145740.3):

T_A: 59 °C / Cycles: 35 / Product size: 185 bp

F: TCTGCCCGTATGTCCACCT

R: GCTCCTCGACGTAGTAGAGAAGT

9 References

Aden, D. P., Fogel, A., Plotkin, S., Damjanov, I., & Knowles, B. B. (1979). Controlled synthesis of HBsAg in a differentiated human liver carcinoma-derived cell line. *Nature, 282*, 615. doi:10.1038/282615a0

Aninat, C., Piton, A., Glaise, D., Le Charpentier, T., Langouët, S., Morel, F., . . . Guillouzo, A. (2006). Expression of cytochromes P450, conjugating enzymes and nuclear receptors in human hepatoma HepaRG cells. *Drug Metab Dispos, 34*(1), 75-83. doi:10.1124/dmd.105.006759

Atale, N., Gupta, S., Yadav, U. C. S., & Rani, V. (2014). Cell-death assessment by fluorescent and nonfluorescent cytosolic and nuclear staining techniques. *Journal of Microscopy, 255*(1), 7-19. doi:10.1111/jmi.12133

Bachmann, A., Moll, M., Gottwald, E., Nies, C., Zantl, R., Wagner, H., . . . Nussler, A. K. (2015). 3D Cultivation Techniques for Primary Human Hepatocytes. *Microarrays (Basel), 4*(1), 64-83. doi:10.3390/microarrays4010064

Bataller, R., & Brenner, D. A. (2005). Liver fibrosis. *The Journal of Clinical Investigation, 115*(2), 209-218. doi:10.1172/JCI24282

Beckwitt, C. H., Clark, A. M., Wheeler, S., Taylor, D. L., Stolz, D. B., Griffith, L., & Wells, A. (2018). Liver 'organ on a chip'. *Exp Cell Res, 363*(1), 15-25. doi:10.1016/j.yexcr.2017.12.023

Berendsen, T. A., Izamis, M. L., Xu, H., Liu, Q., Hertl, M., Berthiaume, F., . . . Uygun, K. (2011). Hepatocyte viability and adenosine triphosphate content decrease linearly over time during conventional cold storage of rat liver grafts. *Transplant Proc, 43*(5), 1484-1488. doi:10.1016/j.transproceed.2010.12.066

Bessems, M., t Hart, N. A., Tolba, R., Doorschodt, B. M., Leuvenink, H. G., Ploeg, R. J., . . . van Gulik, T. M. (2006). The isolated perfused rat liver: standardization of a time-honoured model. *Lab Anim, 40*(3), 236-246. doi:10.1258/002367706777611460

Biosystems, K. (2017). *Wilmington, Massachusetts, USA*.

Bouma, M. E., Pessah, M., Renaud, G., Amit, N., Catala, D., & Infante, R. (1988). Synthesis and secretion of lipoproteins by human hepatocytes in culture. *In Vitro Cell Dev Biol, 24*(2), 85-90. doi:10.1007/bf02623884

Brodniewicz, T., & Grynkiewicz, G. (2010). Preclinical drug development. *Acta Pol Pharm, 67*(6), 578-585.

Brown, J. H., Das, P., DiVito, M. D., Ivancic, D., Tan, L. P., & Wertheim, J. A. (2018). Nanofibrous PLGA electrospun scaffolds modified with type I collagen influence hepatocyte function and support viability in vitro. *Acta Biomater, 73*, 217-227. doi:10.1016/j.actbio.2018.02.009

Carvalho, B. M. A., Da Silva, S. L., Da Silva, L. H. M., Minim, V. P. R., Da Silva, M. C. H., Carvalho, L. M., & Minim, L. A. (2014). Cryogel Poly(acrylamide): Synthesis, Structure and Applications. *Separation & Purification Reviews, 43*(3), 241-262. doi:10.1080/15422119.2013.795902

Castell, J. V., Jover, R., Martínez-Jiménez, C. P., & Gómez-Lechón, M. J. (2006). Hepatocyte cell lines: their use, scope and limitations in drug metabolism studies. *Expert Opin Drug Metab Toxicol, 2*(2), 183-212. doi:10.1517/17425255.2.2.183

Chua, K. N., Lim, W. S., Zhang, P., Lu, H., Wen, J., Ramakrishna, S., . . . Mao, H. Q. (2005). Stable immobilization of rat hepatocyte spheroids on galactosylated nanofiber scaffold. *Biomaterials, 26*(15), 2537-2547. doi:10.1016/j.biomaterials.2004.07.040

Cipriano, M., Correia, J. C., Camões, S. P., Oliveira, N. G., Cruz, P., Cruz, H., . . . Miranda, J. P. (2017). The role of epigenetic modifiers in extended cultures of functional hepatocyte-like cells derived from human neonatal mesenchymal stem cells. *Arch Toxicol, 91*(6), 2469-2489. doi:10.1007/s00204-016-1901-x

Damania, A., Kumar, A., Teotia, A. K., Kimura, H., Kamihira, M., Ijima, H., . . . Kumar, A. (2018). Decellularized Liver Matrix-Modified Cryogel Scaffolds as Potential Hepatocyte Carriers in Bioartificial Liver Support Systems and Implantable Liver Constructs. *ACS Appl Mater Interfaces, 10*(1), 114-126. doi:10.1021/acsami.7b13727

Dambach, D. M., Andrews, B. A., & Moulin, F. (2005). New Technologies and Screening Strategies for Hepatotoxicity: Use of In Vitro Models. *Toxicologic Pathology, 33*(1), 17-26. doi:10.1080/01926230590522284

David, S., & Hamilton, J. P. (2010). Drug-induced Liver Injury. *US Gastroenterol Hepatol Rev, 6*, 73-80.

Dean, M., Hamon, Y., & Chimini, G. (2001). The human ATP-binding cassette (ABC) transporter superfamily. *Journal of lipid research, 42*(7), 1007-1017.

Directive 2001/83/EC of the European Parliament and of the Council of 6 November 2001 on the Community code relating to medicinal products for human use (28/11/2001). *Official journal of the European Union.* L 311. Retrieved from https://eurlex.europa.eu/LexUriServ/LexUriServ.do?uri=CELEX:32001L0083:EN:HTML

Donato, M. T., Jiménez, N., Castell, J. V., & Gómez-Lechón, M. J. (2004). FLUORESCENCE-BASED ASSAYS FOR SCREENING NINE CYTOCHROME P450 (P450) ACTIVITIES IN INTACT CELLS EXPRESSING INDIVIDUAL HUMAN P450 ENZYMES. *Drug Metabolism and Disposition, 32*(7), 699. doi:10.1124/dmd.32.7.699

Donato, M. T., Lahoz, A., Castell, J. V., & Gómez-Lechón, M. J. (2008). Cell lines: a tool for in vitro drug metabolism studies. *Curr Drug Metab, 9*(1), 1-11. doi:10.2174/138920008783331086

Dresser, G. K., Spence, J. D., & Bailey, D. G. (2000). Pharmacokinetic-Pharmacodynamic Consequences and Clinical Relevance of Cytochrome P450 3A4 Inhibition. *Clinical Pharmacokinetics, 38*(1), 41-57. doi:10.2165/00003088-200038010-00003

The Drug Development Process. (2018, 01/04/2018). Retrieved from https://www.fda.gov/patients/learn-about-drug-and-device-approvals/drug-development-process

Dunn, J. C., Yarmush, M. L., Koebe, H. G., & Tompkins, R. G. (1989). Hepatocyte function and extracellular matrix geometry: long-term culture in a sandwich configuration. *The FASEB Journal, 3*(2), 174-177. doi:10.1096/fasebj.3.2.2914628

Dupont, C., Armant, D. R., & Brenner, C. A. (2009). Epigenetics: definition, mechanisms and clinical perspective. *Semin Reprod Med, 27*(5), 351-357. doi:10.1055/s-0029-1237423

Eisenberg, E., & Levanon, E. Y. (2013). Human housekeeping genes, revisited. *Trends in Genetics, 29*(10), 569-574. doi:https://doi.org/10.1016/j.tig.2013.05.010

Elaut, G., Henkens, T., Papeleu, P., Snykers, S., Vinken, M., Vanhaecke, T., & Rogiers, V. (2006). Molecular mechanisms underlying the dedifferentiation process of isolated hepatocytes and their cultures. *Curr Drug Metab, 7*(6), 629-660. doi:10.2174/138920006778017759

Everwien, H., Ariza de Schellenberger, A., Haep, N., Tzschätzsch, H., Pratschke, J., Sauer, I. M., . . . Sack, I. (2020). Magnetic resonance elastography quantification of the solid-to-fluid transition of liver tissue due to decellularization. *Journal of the Mechanical Behavior of Biomedical Materials, 104*, 103640. doi:https://doi.org/10.1016/j.jmbbm.2020.103640

Fan, J., Jia, X., Huang, Y., Fu, B. M., & Fan, Y. (2015). Greater scaffold permeability promotes growth of osteoblastic cells in a perfused bioreactor. *J Tissue Eng Regen Med, 9*(12), E210-218. doi:10.1002/term.1701

Fox, E., Curt, G. A., & Balis, F. M. (2002). Clinical Trial Design for Target-Based Therapy. *The Oncologist, 7*(5), 401-409. doi:10.1634/theoncologist.7-5-401

Gebhardt, R., Hengstler, J. G., Müller, D., Glöckner, R., Buenning, P., Laube, B., . . . Oesch, F. (2003). New hepatocyte in vitro systems for drug metabolism: metabolic capacity and recommendations for application in basic research and drug development, standard operation procedures. *Drug Metab Rev, 35*(2-3), 145-213. doi:10.1081/dmr-120023684

Gerhard Aumüller, G. A., Andreas Doll, Jürgen Engele, Joachim Kirsch, Siegfried Mense, Laurenz J. Wurzinger. (2010). *Duale Reihe: Anatomie* (2nd Edition ed.). Stuttgart: Thieme.

Ghanemi, A. (2015). Cell cultures in drug development: Applications, challenges and limitations. *Saudi pharmaceutical journal : SPJ : the official publication of the Saudi Pharmaceutical Society, 23*(4), 453-454. doi:10.1016/j.jsps.2014.04.002

Giri, S., & Bader, A. (2011). Improved preclinical safety assessment using micro-BAL devices: the potential impact on human discovery and drug attrition. *Drug Discovery Today, 16*(9), 382-397. doi:https://doi.org/10.1016/j.drudis.2011.02.012

Godoy, P., Hengstler, J. G., Ilkavets, I., Meyer, C., Bachmann, A., Müller, A., Dooley, S. (2009). Extracellular matrix modulates sensitivity of hepatocytes to fibroblastoid dedifferentiation and transforming growth factor β–induced apoptosis. *Hepatology, 49*(6), 2031-2043. doi:10.1002/hep.22880

Godoy, P., Hewitt, N. J., Albrecht, U., Andersen, M. E., Ansari, N., Bhattacharya, S., . . . Hengstler, J. G. (2013). Recent advances in 2D and 3D in vitro systems using primary hepatocytes, alternative hepatocyte sources and non-parenchymal liver cells and their use in investigating mechanisms of hepatotoxicity, cell signaling and ADME. *Arch Toxicol, 87*(8), 1315-1530. doi:10.1007/s00204-013-1078-5

Godoy, P., Schug, M., Bauer, A., & Hengstler, J. G. (2010). Reversible manipulation of apoptosis sensitivity in cultured hepatocytes by matrix-mediated manipulation of signaling activities. *Methods Mol Biol, 640*, 139-155. doi:10.1007/978-1-60761-688-7_7

Green, C. J., Charlton, C. A., Wang, L. M., Silva, M., Morten, K. J., & Hodson, L. (2017). The isolation of primary hepatocytes from human tissue: optimising the use of

small non-encapsulated liver resection surplus. *Cell Tissue Bank, 18*(4), 597-604. doi:10.1007/s10561-017-9641-6

Grundbacher, F. J. (1992). Behring's discovery of diphtheria and tetanus antitoxins. *Immunol Today, 13*(5), 188-190. doi:10.1016/0167-5699(92)90125-q

Guguen-Guillouzo, C., & Guillouzo, A. (2010). General review on in vitro hepatocyte models and their applications. *Methods Mol Biol, 640*, 1-40. doi:10.1007/978-1-60761-688-7_1

Häussling, V., Deninger, S., Vidoni, L., Rinderknecht, H., Ruoß, M., Arnscheidt, C., . . . Ehnert, S. (2019). Impact of Four Protein Additives in Cryogels on Osteogenic Differentiation of Adipose-Derived Mesenchymal Stem Cells. *Bioengineering (Basel, Switzerland), 6*(3). doi:10.3390/bioengineering6030067

Hayes, J. D., & Pulford, D. J. (1995). The glutathione S-transferase supergene family: regulation of GST and the contribution of the isoenzymes to cancer chemoprotection and drug resistance. *Crit Rev Biochem Mol Biol, 30*(6), 445-600. doi:10.3109/10409239509083491

Hixon, K. R., Lu, T., & Sell, S. A. (2017). A comprehensive review of cryogels and their roles in tissue engineering applications. *Acta Biomater, 62*, 29-41. doi:10.1016/j.actbio.2017.08.033

Hollister, S. J. (2005). Porous scaffold design for tissue engineering. *Nat Mater, 4*(7), 518-524. doi:10.1038/nmat1421

Horn, F. (2009). *Biochemie des Menschen* (4th Edition ed.). Stuttgart: Thieme.

Huggett, J. F., O'Grady, J., & Bustin, S. (2015). qPCR, dPCR, NGS - A journey. *Biomolecular detection and quantification, 3*, A1-A5. doi:10.1016/j.bdq.2015.01.001

Hughes, C. S., Postovit, L. M., & Lajoie, G. A. (2010). Matrigel: a complex protein mixture required for optimal growth of cell culture. *Proteomics, 10*(9), 1886-1890. doi:10.1002/pmic.200900758

Hussain, A. N., Zafar, M., Ahmad, M., Khan, R., Yaseen, G., Khan, M. S., . . . Shaheen, S. (2018). Comparative SEM and LM foliar epidermal and palyno-morphological studies of Amaranthaceae and its taxonomic implications. *Microsc Res Tech, 81*(5), 474-485. doi:10.1002/jemt.23001

Iandolo, D., Pennacchio, F. A., Mollo, V., Rossi, D., Dannhauser, D., Cui, B., . . . Santoro, F. (2019). Electron Microscopy for 3D Scaffolds-Cell Biointerface Characterization. *Advanced biosystems, 3*(2), e1800103-e1800103. doi:10.1002/adbi.201800103

Jain, E., Damania, A., Shakya, A. K., Kumar, A., Sarin, S. K., & Kumar, A. (2015). Fabrication of macroporous cryogels as potential hepatocyte carriers for bioartificial liver support. *Colloids Surf B Biointerfaces, 136*, 761-771. doi:10.1016/j.colsurfb.2015.10.012

Jancova, P., Anzenbacher P Fau - Anzenbacherova, E., & Anzenbacherova, E. Phase II drug metabolizing enzymes. (1213-8118 (Print)).

Jankovic, S. M., Kapo, B., Sukalo, A., & Masic, I. (2019). Evaluation of Published Preclinical Experimental Studies in Medicine: Methodology Issues. *Med Arch, 73*(5), 298-302. doi:10.5455/medarh.2019.73.298-302

Jones, L. J., Gray, M., Yue, S. T., Haugland, R. P., & Singer, V. L. (2001). Sensitive determination of cell number using the CyQUANT® cell proliferation assay. *Journal of Immunological Methods, 254*(1), 85-98. doi:https://doi.org/10.1016/S0022-1759(01)00404-5

Jung, D., Biggs, H., Erikson, J., & Ledyard, P. U. (1975). New Colorimetric Reaction for End-Point, Continuous-Flow, and Kinetic Measurement of Urea. *Clinical Chemistry, 21*(8), 1136-1140. doi:10.1093/clinchem/21.8.1136

Kanwal, R., & Gupta, S. (2012). Epigenetic modifications in cancer. *Clinical Genetics, 81*(4), 303-311. doi:10.1111/j.1399-0004.2011.01809.x

Kidambi, S., Yarmush, R. S., Novik, E., Chao, P., Yarmush, M. L., & Nahmias, Y. (2009). Oxygen-mediated enhancement of primary hepatocyte metabolism, functional polarization, gene expression, and drug clearance. *Proceedings of the National Academy of Sciences, 106*(37), 15714. doi:10.1073/pnas.0906820106

Kietzmann, T. (2017). Metabolic zonation of the liver: The oxygen gradient revisited. *Redox Biol, 11*, 622-630. doi:10.1016/j.redox.2017.01.012

Kilic Bektas, C., & Hasirci, V. (2019). Cell Loaded GelMA:HEMA IPN hydrogels for corneal stroma engineering. *J Mater Sci Mater Med, 31*(1), 2. doi:10.1007/s10856-019-6345-4

Kimura, H., Sakai, Y., & Fujii, T. (2018). Organ/body-on-a-chip based on microfluidic technology for drug discovery. *Drug Metab Pharmacokinet, 33*(1), 43-48. doi:10.1016/j.dmpk.2017.11.003

Kizawa, H., Nagao, E., Shimamura, M., Zhang, G., & Torii, H. (2017). Scaffold-free 3D bio-printed human liver tissue stably maintains metabolic functions useful for drug discovery. *Biochem Biophys Rep, 10*, 186-191. doi:10.1016/j.bbrep.2017.04.004

Koike, M., Matsushita, M., Taguchi, K., & Uchino, J. (1996). Function of culturing monolayer hepatocytes by collagen gel coating and coculture with nonparenchymal cells. *Artif Organs, 20*(2), 186-192. doi:10.1111/j.1525-1594.1996.tb00725.x

Kost, D. P., & Michalopoulos, G. K. (1991). Effect of 2% dimethyl sulfoxide on the mitogenic properties of epidermal growth factor and hepatocyte growth factor in primary hepatocyte culture. *J Cell Physiol, 147*(2), 274-280. doi:10.1002/jcp.1041470212

Kumar, A., & Jaitak, V. (2019). Natural products as multidrug resistance modulators in cancer. *Eur J Med Chem, 176*, 268-291. doi:10.1016/j.ejmech.2019.05.027

Kumari, J., Karande, A. A., & Kumar, A. (2016). Combined Effect of Cryogel Matrix and Temperature-Reversible Soluble-Insoluble Polymer for the Development of in Vitro Human Liver Tissue. *ACS Appl Mater Interfaces, 8*(1), 264-277. doi:10.1021/acsami.5b08607

Lee, M.-K., & Kim, H.-R. (2006). Comparison between Real-Time PCR and Agarose Gel Electrophoresis for DNA Quantification. *Annals of Laboratory Medicine, 26*(3), 217-222. doi:10.3343/kjlm.2006.26.3.217

Leist, M., & Hartung, T. (2013). Inflammatory findings on species extrapolations: humans are definitely no 70-kg mice. *Arch Toxicol, 87*(4), 563-567. doi:10.1007/s00204-013-1038-0

Lim, J. S. L., Chen, X. A., Singh, O., Yap, Y. S., Ng, R. C. H., Wong, N. S., . . . Chowbay, B. (2011). Impact of CYP2D6, CYP3A5, CYP2C9 and CYP2C19 polymorphisms on tamoxifen pharmacokinetics in Asian breast cancer patients. *British Journal of Clinical Pharmacology, 71*(5), 737-750. doi:10.1111/j.1365-2125.2011.03905.x

Lin, J., Schyschka, L., Mühl-Benninghaus, R., Neumann, J., Hao, L., Nussler, N., . . . Ehnert, S. (2012). Comparative analysis of phase I and II enzyme activities in 5 hepatic cell lines identifies Huh-7 and HCC-T cells with the highest potential to

study drug metabolism. *Archives of Toxicology, 86*(1), 87-95. doi:10.1007/s00204-011-0733-y

Liu, Z., Tamaddon, M., Gu, Y., Yu, J., Xu, N., Gang, F., . . . Liu, C. (2020). Cell Seeding Process Experiment and Simulation on Three-Dimensional Polyhedron and Cross-Link Design Scaffolds. *Frontiers in bioengineering and biotechnology, 8*, 104-104. doi:10.3389/fbioe.2020.00104

Louisse, J., de Jong, E., van de Sandt, J. J. M., Blaauboer, B. J., Woutersen, R. A., Piersma, A. H., . . . Verwei, M. (2010). The Use of In Vitro Toxicity Data and Physiologically Based Kinetic Modeling to Predict Dose-Response Curves for In Vivo Developmental Toxicity of Glycol Ethers in Rat and Man. *Toxicological Sciences, 118*(2), 470-484. doi:10.1093/toxsci/kfq270

Lu, J. F., Pokharel, D., & Bebawy, M. (2015). MRP1 and its role in anticancer drug resistance. *Drug Metabolism Reviews, 47*(4), 406-419. doi:10.3109/03602532.2015.1105253

Luckert, C., Schulz, C., Lehmann, N., Thomas, M., Hofmann, U., Hammad, S., . . . Hessel, S. (2017). Comparative analysis of 3D culture methods on human HepG2 cells. *Archives of Toxicology, 91*(1), 393-406. doi:10.1007/s00204-016-1677-z

Marone, M., Mozzetti, S., De Ritis, D., Pierelli, L., & Scambia, G. (2001). Semiquantitative RT-PCR analysis to assess the expression levels of multiple transcripts from the same sample. *Biological procedures online, 3*, 19-25. doi:10.1251/bpo20

Mattei, G., Magliaro, C., Pirone, A., & Ahluwalia, A. (2018). Bioinspired liver scaffold design criteria. *Organogenesis, 14*(3), 129-146. doi:10.1080/15476278.2018.1505137

Melke, J., Zhao, F., Ito, K., & Hofmann, S. (2020). Orbital seeding of mesenchymal stromal cells increases osteogenic differentiation and bone-like tissue formation. *Journal of Orthopaedic Research, 38*(6), 1228-1237. doi:10.1002/jor.24583

Meng, D., Lei, X., Li, Y., Kong, Y., Huang, D., & Zhang, G. (2020). Three dimensional polyvinyl alcohol scaffolds modified with collagen for HepG2 cell culture. *Journal of Biomaterials Applications, 35*(4-5), 459-470. doi:10.1177/0885328220933505

Mikos, A., & Temenoff, J. (2000). Formation of highly porous biodegradable scaffolds for tissue engineering. *Electronic Journal of Biotechnology (Chile) Num.2 Vol.3, 3*. doi:10.2225/vol3-issue2-fulltext-5

Mirzaeian, L., Eivazkhani, F., Hezavehei, M., Moini, A., Esfandiari, F., Valojerdi, M. R., & Fathi, R. (2020). Optimizing The Cell Seeding Protocol to Human Decellularized Ovarian Scaffold: Application of Dynamic System for Bio-Engineering. *Cell journal, 22*(2), 227-235. doi:10.22074/cellj.2020.6604

Mizutani, R., & Suzuki, Y. (2012). X-ray microtomography in biology. *Micron, 43*(2), 104-115. doi:https://doi.org/10.1016/j.micron.2011.10.002

Naeem, E. M., Sajad, D., Talaei-Khozani, T., Khajeh, S., Azarpira, N., Alaei, S., . . . Razban, V. (2019). Decellularized liver transplant could be recellularized in rat partial hepatectomy model. *Journal of Biomedical Materials Research Part A, 107*(11), 2576-2588. doi:https://doi.org/10.1002/jbm.a.36763

Nagaki, M., Miki, K., Kim, Y. I., Ishiyama, H., Hirahara, I., Takahashi, H., . . . Moriwaki, H. (2001). Development and characterization of a hybrid bioartificial liver using

primary hepatocytes entrapped in a basement membrane matrix. *Dig Dis Sci, 46*(5), 1046-1056. doi:10.1023/a:1010714112675

Oelschlaeger, C., Bossler, F., & Willenbacher, N. (2016). Synthesis, Structural and Micromechanical Properties of 3D Hyaluronic Acid-Based Cryogel Scaffolds. *Biomacromolecules, 17*(2), 580-589. doi:10.1021/acs.biomac.5b01529

Onakpoya, I. J., Heneghan, C. J., & Aronson, J. K. (2016). Post-marketing withdrawal of 462 medicinal products because of adverse drug reactions: a systematic review of the world literature. *BMC Med, 14*, 10. doi:10.1186/s12916-016-0553-2

Pan, M. X., Cheng, Y., Wang, Y., He, G. L., Hu, P. Y., & Gao, Y. (2011). [Preparation of a decellularized rat liver scaffold and its biocompatibility]. *Nan Fang Yi Ke Da Xue Xue Bao, 31*(1), 69-72.

Park, B. H., Han, Y. A., Choi, J. H., & Lim, J. O. (2004). Biocompatibility of Phema and P(Hema-Co-Sma) Hydrogels. *Key Engineering Materials, 277-279*, 51-55. doi:10.4028/www.scientific.net/KEM.277-279.51

Patel, K., & Wilder, J. (2014). Fibroscan. *Clinical liver disease, 4*(5), 97-101. doi:10.1002/cld.407

Prestwich, G. D. (2008). Evaluating drug efficacy and toxicology in three dimensions: using synthetic extracellular matrices in drug discovery. *Acc Chem Res, 41*(1), 139-148. doi:10.1021/ar7000827

Ramaiahgari, S. C., den Braver, M. W., Herpers, B., Terpstra, V., Commandeur, J. N. M., van de Water, B., & Price, L. S. (2014). A 3D in vitro model of differentiated HepG2 cell spheroids with improved liver-like properties for repeated dose high-throughput toxicity studies. *Archives of Toxicology, 88*(5), 1083-1095. doi:10.1007/s00204-014-1215-9

Roberts, R. A., Ganey, P. E., Ju, C., Kamendulis, L. M., Rusyn, I., & Klaunig, J. E. (2006). Role of the Kupffer Cell in Mediating Hepatic Toxicity and Carcinogenesis. *Toxicological Sciences, 96*(1), 2-15. doi:10.1093/toxsci/kfl173

Romano, V., Parekh, M., Ruzza, A., Willoughby, C. E., Ferrari, S., Ponzin, D., . . . Levis, H. J. (2018). Comparison of preservation and transportation protocols for preloaded Descemet membrane endothelial keratoplasty. *British Journal of Ophthalmology, 102*(4), 549. doi:10.1136/bjophthalmol-2017-310906

Ruoß, Damm, G., Vosough, M., Ehret, L., Grom-Baumgarten, C., Petkov, M., . . . Sajadian, S. (2019). Epigenetic Modifications of the Liver Tumor Cell Line HepG2 Increase Their Drug Metabolic Capacity. *Int J Mol Sci, 20*(2). doi:10.3390/ijms20020347

Ruoß, M., Häussling, V., Schügner, F., Olde Damink, L. H. H., Lee, S. M. L., Ge, L., . . . Nussler, A. K. (2018). A Standardized Collagen-Based Scaffold Improves Human Hepatocyte Shipment and Allows Metabolic Studies over 10 Days. *Bioengineering (Basel, Switzerland), 5*(4), 86. doi:10.3390/bioengineering5040086

Ruoß, M., Kieber, V., Rebholz, S., Linnemann, C., Rinderknecht, H., Häussling, V., . . . Nussler, A. K. (2019). Cell-Type-Specific Quantification of a Scaffold-Based 3D Liver Co-Culture. *Methods and protocols, 3*(1), 1. doi:10.3390/mps3010001

Ruoß, M., Rebholz, S., Weimer, M., Grom-Baumgarten, C., Athanasopulu, K., Kemkemer, R., . . . Nussler, A. K. (2020). Development of Scaffolds with Adjusted Stiffness for Mimicking Disease-Related Alterations of Liver Rigidity. *J Funct Biomater, 11*(1). doi:10.3390/jfb11010017

Sajadian, S. O., Ehnert, S., Vakilian, H., Koutsouraki, E., Damm, G., Seehofer, D., . . . Nussler, A. K. (2015). Induction of active demethylation and 5hmC formation by 5-azacytidine is TET2 dependent and suggests new treatment strategies against hepatocellular carcinoma. *Clinical Epigenetics, 7*(1), 98. doi:10.1186/s13148-015-0133-x

Sajadian, S. O., Tripura, C., Samani, F. S., Ruoss, M., Dooley, S., Baharvand, H., & Nussler, A. K. (2016). Vitamin C enhances epigenetic modifications induced by 5-azacytidine and cell cycle arrest in the hepatocellular carcinoma cell lines HLE and Huh7. *Clin Epigenetics, 8*, 46. doi:10.1186/s13148-016-0213-6

Sambrook, J., Fritsch, E. F., & Maniatis, T. (1989). *Molecular cloning: a laboratory manual*: Cold spring harbor laboratory press.

Schubert-Zsilavecz, M. (2011, 25.07.2011). Arzneimittelrücknahmen: Rückrufe im Rückblick. *Pharmazeutische Zeitung*. Retrieved from https://www.pharmazeutische-zeitung.de/ausgabe-302011/rueckrufe-im-rueckblick/

Schyschka, L., Sánchez, J. J. M., Wang, Z., Burkhardt, B., Müller-Vieira, U., Zeilinger, K., . . . Nussler, A. K. (2013). Hepatic 3D cultures but not 2D cultures preserve specific transporter activity for acetaminophen-induced hepatotoxicity. *Archives of Toxicology, 87*(8), 1581-1593. doi:10.1007/s00204-013-1080-y

Seeliger, C., Culmes, M., Schyschka, L., Yan, X., Damm, G., Wang, Z., . . . Nüssler, A. K. (2013). Decrease of Global Methylation Improves Significantly Hepatic Differentiation of Ad-MSCs: Possible Future Application for Urea Detoxification. *Cell Transplantation, 22*(1), 119-131. doi:10.3727/096368912X638946

Shimizu, K., Ito, A., & Honda, H. (2006). Enhanced cell-seeding into 3D porous scaffolds by use of magnetite nanoparticles. *J Biomed Mater Res B Appl Biomater, 77*(2), 265-272. doi:10.1002/jbm.b.30443

Sinha, M., Dhawan, A., & Parthasarathi, R. (2019). In Silico Approaches in Predictive Genetic Toxicology. *Methods Mol Biol, 2031*, 351-373. doi:10.1007/978-1-4939-9646-9_20

Sison-Young, R. L., Lauschke, V. M., Johann, E., Alexandre, E., Antherieu, S., Aerts, H., . . . Park, B. K. (2017). A multicenter assessment of single-cell models aligned to standard measures of cell health for prediction of acute hepatotoxicity. *Archives of Toxicology, 91*(3), 1385-1400. doi:10.1007/s00204-016-1745-4

Skehan, P., Storeng, R., Scudiero, D., Monks, A., McMahon, J., Vistica, D., . . . Boyd, M. R. (1990). New Colorimetric Cytotoxicity Assay for Anticancer-Drug Screening. *JNCI: Journal of the National Cancer Institute, 82*(13), 1107-1112. doi:10.1093/jnci/82.13.1107

Song, J. J., Guyette, J. P., Gilpin, S. E., Gonzalez, G., Vacanti, J. P., & Ott, H. C. (2013). Regeneration and experimental orthotopic transplantation of a bioengineered kidney. *Nature Medicine, 19*(5), 646-651. doi:10.1038/nm.3154

Stewart, N. T., Byrne, K. M., Hosick, H. L., Vierck, J. L., & Dodson, M. V. (2000). Traditional and emerging methods for analyzing cell activity in cell culture. *Methods in Cell Science, 22*(1), 67-78. doi:10.1023/A:1009839501174

Stol, M., Tolar, M., & Adam, M. (1985). Poly(2-hydroxyethyl methacrylate)--collagen composites which promote muscle cell differentiation in vitro. *Biomaterials, 6*(3), 193-197. doi:10.1016/0142-9612(85)90009-2

Stravitz, R. T., & Lee, W. M. Acute liver failure. (1474-547X (2019)).

Teng, F., Ding, H., Huang, Y., & Wang, J. (2018). Fabrication of three-dimensional nanofibrous gelatin scaffolds using one-step crosslink technique. *J Biomater Sci Polym Ed, 29*(15), 1859-1875. doi:10.1080/09205063.2018.1515299

Thermo Fisher Scientific, W., USA. (2017).

Treyer, A., & Müsch, A. (2013). Hepatocyte Polarity. *Comprehensive Physiology, 3*, 243-287. doi:10.1002/cphy.c120009

Uzarski, J. S., DiVito, M. D., Wertheim, J. A., & Miller, W. M. (2017). Essential design considerations for the resazurin reduction assay to noninvasively quantify cell expansion within perfused extracellular matrix scaffolds. *Biomaterials, 129*, 163-175. doi:10.1016/j.biomaterials.2017.02.015

van Tonder, A., Joubert, A. M., & Cromarty, A. D. (2015). Limitations of the 3-(4,5-dimethylthiazol-2-yl)-2,5-diphenyl-2H-tetrazolium bromide (MTT) assay when compared to three commonly used cell enumeration assays. *BMC research notes, 8*, 47-47. doi:10.1186/s13104-015-1000-8

Vecchio, I., Tornali, C., Bragazzi, N. L., & Martini, M. (2018). The Discovery of Insulin: An Important Milestone in the History of Medicine. *Frontiers in Endocrinology, 9*(613). doi:10.3389/fendo.2018.00613

Wang, S., Nagrath, D., Chen, P. C., Berthiaume, F., & Yarmush, M. L. (2008). Three-Dimensional Primary Hepatocyte Culture in Synthetic Self-Assembling Peptide Hydrogel. *Tissue Engineering Part A, 14*(2), 227-236. doi:10.1089/tea.2007.0143

Wang, X., Ai, A., Yu, Z., Deng, M., Liu, W., Zhou, G., . . . Wang, X. (2020). Dual-modal non-invasive imaging in vitro and in vivo monitoring degradation of PLGA scaffold based gold nanoclusters. *Mater Sci Eng C Mater Biol Appl, 107*, 110307. doi:10.1016/j.msec.2019.110307

Wang, Y., Liu, H., Zhang, M., Wang, H., Chen, W., & Qin, J. (2020). One-step synthesis of composite hydrogel capsules to support liver organoid generation from hiPSCs. *Biomater Sci*. doi:10.1039/d0bm01085e

Wei, J., Lei, D., Chen, M., Ran, P., & Li, X. (2020). Engineering HepG2 spheroids with injectable fiber fragments as predictable models for drug metabolism and tumor infiltration. *J Biomed Mater Res B Appl Biomater*. doi:10.1002/jbm.b.34669

Westerink, W. M. A., & Schoonen, W. G. E. J. (2007a). Cytochrome P450 enzyme levels in HepG2 cells and cryopreserved primary human hepatocytes and their induction in HepG2 cells. *Toxicology in Vitro, 21*(8), 1581-1591. doi:https://doi.org/10.1016/j.tiv.2007.05.014

Westerink, W. M. A., & Schoonen, W. G. E. J. (2007b). Phase II enzyme levels in HepG2 cells and cryopreserved primary human hepatocytes and their induction in HepG2 cells. *Toxicology in Vitro, 21*(8), 1592-1602. doi:https://doi.org/10.1016/j.tiv.2007.06.017

Wichterle, O., & LÍM, D. (1960). Hydrophilic Gels for Biological Use. *Nature, 185*(4706), 117-118. doi:10.1038/185117a0

Wilkening, S., Stahl, F., & Bader, A. (2003). COMPARISON OF PRIMARY HUMAN HEPATOCYTES AND HEPATOMA CELL LINE HEPG2 WITH REGARD TO THEIR BIOTRANSFORMATION PROPERTIES. *Drug Metabolism and Disposition, 31*(8), 1035-1042. doi:10.1124/dmd.31.8.1035

Xia, T., Zhao, R., Feng, F., & Yang, L. (2020). The Effect of Matrix Stiffness on Human Hepatocyte Migration and Function-An In Vitro Research. *Polymers, 12*(9), 1903. doi:10.3390/polym12091903

Zawada, R. J. X., Kwan, P., Olszewski, K. L., Llinas, M., & Huang, S.-G. (2009). Quantitative determination of urea concentrations in cell culture medium. *Biochemistry and Cell Biology, 87*(3), 541-544. doi:10.1139/O09-011

Zhang, Y., Wang, Q. S., Yan, K., Qi, Y., Wang, G. F., & Cui, Y. L. (2016). Preparation, characterization, and evaluation of genipin crosslinked chitosan/gelatin three-dimensional scaffolds for liver tissue engineering applications. *J Biomed Mater Res A, 104*(8), 1863-1870. doi:10.1002/jbm.a.35717

Zhou, S.-F., Wang, B., Yang, L.-P., & Liu, J.-P. (2010). Structure, function, regulation and polymorphism and the clinical significance of human cytochrome P450 1A2. *Drug Metabolism Reviews, 42*(2), 268-354. doi:10.3109/03602530903286476

Zhu, W., Ma, X., Gou, M., Mei, D., Zhang, K., & Chen, S. (2016). 3D printing of functional biomaterials for tissue engineering. *Curr Opin Biotechnol, 40*, 103-112. doi:10.1016/j.copbio.2016.03.014

Zimmermann, S., Gretzinger, S., Scheeder, C., Schwab, M.-L., Oelmeier, S. A., Osberghaus, A., . . . Hubbuch, J. (2016). High-throughput cell quantification assays for use in cell purification development – enabling technologies for cell production. *Biotechnology Journal, 11*(5), 676-686. doi:https://doi.org/10.1002/biot.201500577

Erklärung zum Eigenanteil

Die Arbeit wurde im Siegfried-Weller-Institut für unfallchirurgische Forschung unter Betreuung von Prof. Dr. rer. nat. Andreas K. Nüssler durchgeführt.

Die Konzeption der Studie erfolgte in Zusammenarbeit mit Dr. rer. nat. Marc Ruoß und Prof. Dr. rer. nat. Andreas K. Nüssler.

Die Versuche wurden nach Einarbeitung durch Marc Ruoß von mir in Zusammenarbeit mit Marc Ruoß durchgeführt. Die Isolierung des Rattenschwanz-Kollagens wurde von Marc Ruoß durchgeführt

Die statistische Auswertung erfolgte nach Beratung durch das Institut für Klinische Epidemiologie und angewandte Biometrie, Universität Tübingen unter Anleitung durch Dr. rer. nat. Marc Ruoß und durch mich.

Ich versichere, das Manuskript verfasst zu haben und keine weiteren als die von mir angegebenen Quellen verwendet zu haben.

Tübingen, den 14.11.2023

Carl Grom-
Baumgarten

Acknowledgements

Foremost, I would like to express my sincere gratitude to my advisor, Prof. Dr. rer. nat. A.K. Nüssler for the continuous support of my doctoral thesis and his immense patience, motivation, and incredible knowledge.

Besides my advisor, I would like to thank Dr. Marc Ruoß for answering all my question, patiently giving explanations and supporting me in finding my way through the topic.

My thanks also go to my laboratory colleagues during my time at the Siegfried-Weller - Institut for their support, advice, and company.

I want to thank my family for their everlasting support throughout my studies and my life.

I also want to thank my wife WMinakshi for her love, support, and her ability to always see the best in every situation and her inexorable efforts to make me see it too.